Ecological successions of rudist communities: A sedimentological and palaeoecological analysis of upper Cenomanian rudist assemblages from the South-Provence Carbonate Platform (SE France)

Valentin Rineau, Marc Floquet, Loïc Villier, Philippe Leonide, Aurélien Blénet, Anna Perla Ackouala Mfere

HAL Id: hal-03518586

https://hal.sorbonne-universite.fr/hal-03518586v1

Submitted on 16 Oct 2023

Ecological successions of rudist communities: a sedimentological and palaeoecological analysis of upper Cenomanian rudist assemblages from the South-Provence Carbonate Platform (SE France)

[1,2]Valentin Rineau*, [3]Marc Floquet, [2]Loïc Villier, [3]Philippe Léonide, [4]Aurélien Blénet and [5]Ana-Perla Ackouala

[1] Charles University, Center for Theoretical Study, Husova 4, 110 00 Praha 1, Czech Republic

[2] Sorbonne Université, Centre de Recherche en Paléontologie - Paris (UMR 7207 CR2P), 4 place Jussieu, barre 46-56 5ème étage, case 104, 75005 Paris, France

[3] Aix-Marseille Université, UM 34 CNRS, IRD, INRAE, Collège de France, CEREGE, Centre Saint-Charles, 3 place Victor Hugo, Case 67, 13331 Marseille, Cedex 03, France

[4] FLODIM, Technoparc des Grandes Terres, 110 rue des Rizières, 04100 Manosque, France.

[5] Université Marien Ngouabi, Département de Géologie BP69, Brazzaville, Congo.

*Corresponding author. Email: valentin.rineau@gmail.fr

Abstract

Carbonate platforms developed in the southwestern Provence area during the late Cretaceous on the rims of a narrow deep E-W oriented basin. The upper Cenomanian lower Member Fontblanche 1 of the Fontblanche Limestones Formation is exceptionally rich in rudists. This member is well exposed in two quarries with flat outcrop surfaces, thanks to sawn surfaces, that allow 3D investigation of its litho- and biofacies and sedimentary structures. The paper describes the sedimentary sequences of each quarry from a quantitative study of both sedimentary and palaeontological data, both macroscopic and microscopic, derived from quadra counts in the field and thin section analyses. The sequences are one to several metres thick and each of them shows a basal drowning and a final emersion surface with evidence of reworking and dissolution. The microfacies are dominated by floatstone texture, most common grains being bioclasts derived from biocorrosion of rudist shells and benthic foraminifers. The matrix is made mostly of microbioclasts and micrite, resulting from a strong microborers activity. Fossil organisms are regarded as autochthonous or parautochthonous. The overall depositional environment was shallow marine with a maximum depth of a few metres in an inner, peritidal, sheltered and quiet platform. We found a link between the sedimentary facies and rudist ecotypes. The statistical analysis of the fossil counts, using multivariate statistics and clustering, differentiates four fossil assemblages, namely the *Chondrodonta* assemblage, the *Apricardia*-Sauvagesiinae assemblage, the *Caprotina* assemblage, and the *Nerinea* assemblage, which are considered to represent biotic communities. The replacement of communities through Fontblanche 1 and within the elementary sequences illustrates a relationship between the benthic communities, the degree of biocorrosion, the sedimentary texture, and the sedimentation rate so that ecological processes affect the sedimentary dynamics which in turn affects communities through feedback mechanism. Such an intimate link between the sedimentary facies and ecosystems

provides evidence that biotic parameters played an important role in the rudist-rich facies succession.

1. Introduction

During the Cretaceous, rudists were dominant bivalve taxa living in warm, shallow waters on carbonate platforms on the Atlantic, Pacific, and Tethyan margins (Masse et al., 1981; Ross and Skelton, 1993; Gili et al., 1995; Skelton et al., 2000; Steuber and Löser, 2000). Because of their diversity and abundance, they were the main producers of carbonate sediments of their time, partly controlling the growth of the carbonate platforms (Floquet, 1982, 1991; Carannante et al., 1993, 1997, 2000; Scott, 1995; Ruberti, 1997; Gili and Skelton, 2000). Their development was punctuated by several episodes of diversification throughout the Cretaceous and by appearance of new lifestyles (Philip, 1981; Masse and Montaggioni, 2001). The number of rudist taxa was linked to the extent of the carbonate platforms (Steuber and Löser, 2000). In a general way, a stepwise increase in the number of taxa took place throughout the Cretaceous with a succession of crises and evolutionary radiations. The rudists faced several biotic crises, the main ones being the two Cretaceous Oceanic Anoxic Events and the Cretaceous-Paleogene extinction event which led to their definitive extinction.

The Cenomanian is characterised by a major increase in the number of rudist taxa, with 32 recorded genera (Steuber et al., 2016). The taxonomic diversification of rudists is probably triggered by the partitioning and by the expansion of carbonate platforms (Steuber et al., 2016), the emergence of new adaptive groups (Skelton, 1978; Steuber and Löser, 2000), and the differentiation of various biotic communities (Fenerci-Masse et al., 2005). A biotic community, or biocenosis, is defined by a set of organisms living in interdependence (Möbius, 1877). It is characterised by an assemblage of taxa present in stable proportions in a given area. During the Cenomanian, rudist communities were abundant, taxonomically and ecologically diverse, particularly on Tethyan margins. Cenomanian communities gathered various rudist ecotypes, partly defined by the orientation of their commissure which was dependent on sea currents (Gili and Götz, 2018) and by the nature of the substrate: elevators

(e.g., *Sauvagesia*), clingers (e.g., *Apricardia*), large spaced recumbents (e.g., *Caprinula*), or encrusting (e.g., *Caprotina*). The Cenomanian was therefore a key period in understanding the evolution of the rudists from a synecological perspective. The evolution of rudist communities was driven by various parameters, such as bathymetry, hydrodynamics, turbidity, salinity, water chemistry, temperature, sedimentation rate, substratum type, or biological interactions.

Rudists are numerous and well identifiable in the late Cenomanian carbonate deposits of the South-Provence Basin (Philip, 1970). The changes in rudist assemblage composition are related to faciologic evolution and sedimentary sequences (Floquet et al., 2013). The assemblages are therefore ideal for understanding the relationships of rudists to their ecosystems. Thus, the purpose of this article is both to precisely define the upper Cenomanian biotic communities of the South-Provence carbonate platform and to infer the dynamic relations of their constituting rudist taxa within an ecosystem. To reach this aim, we focus the investigation on two close sections with slightly different sedimentary records. Each section is described by quantitative litho-biofacies analyses of thin sections, and by identification of biotic communities from taxon occurrence counts in the field. Then, the successions of biotic assemblages can be linked to the facies evolution, and the relations between biotic communities to their environment explored in terms of ecological dynamics.

2. Geological and geographical settings

The middle Cenomanian to upper Santonian South-Provence Basin (Fig. 1A, B) was a N-S narrowed (from 25 up to 50 km according to the period) and E-W elongated basin (total extension unknown but at least 80 km long) that comprised two parts: i) to the south, a relatively deep basin (Basin *s.s.* in Fig. 1C) with mixed sediments, siliciclastic and carbonated from heterozoan biotic association of circalittoral environments, and ii) to the north and east, a shallow carbonate platform (Fig. 1C) of infralittoral environments with chlorozoan biotic association including numerous rudists (Philip, 1970, 1972, 1993; Floquet et al., 2018). The

South-Provence Basin was rimmed by two emerged lands: the 'Meridional Massif' to the south (Fig. 1C) (Redondo, 1986; Floquet and Hennuy, 2003; Hennuy, 2003) that yielded siliciclastic supplies to the basin; and the emerged 'Durancian High' to the north (Fig. 1C) (Masse and Philip, 1976) where bauxite was produced by carbonate alteration. The South-Provence Basin was a northern marginal element of the large Pyrenean-Provencal Rift which was connecting the Atlantic Oceanic domain to the west and the Alpine Valaisan basin to the east (Floquet and Hennuy, 2001, 2003; Hennuy, 2003; Floquet et al., 2005, 2006), considering that the South-Provence Basin probably communicated with the alpine Vocontian Basin to the east since the late Cenomanian (Fig. 1B, C).

In southwestern Provence, the late Cenomanian to earliest Turonian rudist-rich carbonate platforms are essentially represented by the Fontblanche Limestones Formation (Philip, 1967, 1978; Floquet et al., 2018) also named 'Calcaires de Fontblanche' or 'Deuxième Barre à Rudistes' (Philip, 1970, 1978). This formation is subdivided into two distinct units: the Fontblanche 1 Unit of the late Cenomanian and the Fontblanche 2 Unit of latest Cenomanian to earliest Turonian age, separated by an unconformity surface (Floquet et al., 2018; Floquet, 2020). Fontblanche 1 corresponds to the upper part of the third-order depositional sequence 2 *sensu* Philip (1998) and to the upper part of the depositional sequence S2 *sensu* Floquet et al. (2018) and Floquet (2020). Fontblanche 2 corresponds to the whole third-order depositional sequence 3 *sensu* Philip (1998) and to the lower part of the depositional sequence S3 *sensu* Floquet et al. (2018) and Floquet (2020). Fontblanche 2 is topped by an unconformity (hardground or firmground) above which nodular clayed limestones develop and yield ammonites of late-early Turonian age (Nodosoides Zone); this unconformity being regarded as a major flooding surface (Crumière-Airaud, 1991; Floquet, 2020). Fontblanche 1 is particularly rich in various rudists and commensal organisms, while Fontblanche 2 exhibits

6

both a sharp decline in biodiversity (of rudist and other taxa) and the appearance of the first hippuritids (Philip, 1978, 1998; Philip et al., 1989).

Two sections were studied in detail, one in the Bastide d'Orves (Fig. 2) and one in the Barre des Aiguilles (Fig. 3) because of the excellent outcrop conditions and of the exceptional rudist richness of Fontblanche 1 there. The upper part of Fontblanche 1 plus Fontblanche 2 were only studied in the Bastide d'Orves section, since the lower part of Fontblanche 1 is not exposed there. The entire Fontblanche 1 plus Fontblanche 2 were studied in the Barre des Aiguilles section. Note that the base of the upper Cenomanian sequences composed of lignitic sandstones and clays, and of rudist and *Praealveolina* bearing quartzose calcarenites ('Gardonian' facies *sensu* Philip, 1970), about 12 m thick, above which the Fontblanche 1 limestones lay, were not detailed in this study because no counting was possible there. Both sections are located in the township of Evenos (Var department, SE France; the Bastide d'Orves one situated at 43°12'5.59"N - 5°54'2.12"E; the Barre des Aiguilles one at 43°10'30.13"N - 5°50'23.41"E).

These sections crop out in the southeastern part of the Beausset syncline that corresponds roughly to the eastern part of the late Cretaceous South-Provence Basin (Fig. 1). More precisely inside the South-Provence Basin, Fontblanche 1 in both sections is representative of inner and predominantly quiet environments of a shallow carbonate platform (Bastide d'Orves and Barre des Aiguilles within the light blue strip in Fig. 1C) which have favoured the development of rudist communities (Floquet, 2020). Conversely, Fontblanche 2 is representative of outer environments, especially in the Bastide d'Orves area, and opened towards the relatively deeper basin (green in Fig. 1C).

3. Material and methods

As the limestones in both quarries were exploited by wire sawing. The resulting surfaces were slick and allow us to easily identify the biofacies and lithofacies, particularly the textural arrangement, and the various fossils. Fossil occurrences were counted directly on the field.

Biosedimentological analyses were carried out both from macrofacies and microfacies, the latter having been studied on 34 thin sections from the Bastide d'Orves quarry (a1 to a34 in Fig. 2) and 42 thin sections from the Barre des Aiguilles quarry (b1 to b42 in Fig. 3), this enabling to characterise the depositional environments and their evolution. Each sample was described based on its texture according to Embry and Klovan (1971) classification and of its micropalaeontological content. The frequencies of the different grain types, mainly bioclasts, were estimated using jmicrovision software 1.2.7 (Roduit, 2008) by counting 250 points randomly distributed on each sample microscope photography. Bioclasts are defined here as the visible grains less than 2 cm in size but that can be taxonomically identified, while microbioclasts correspond to grains generally less than 30 μm in size, only visible under a microscope and taxonomically unidentifiable.

The bioclastic fraction (Figs. 2, 3) is defined as the ratio between the percentage of bioclasts ranging between 30 μm and 2 cm and the percentage of matrix (microbioclastic and micritic) or cement (microsparite, sparite). The similarity/difference of facies was statistically tested by ANOVA correlation. The independence between absence/presence of specific taxa and sedimentary features was tested by a Fischer's exact test. The correlation between the bioclastic fraction and the species richness was tested through the Pearson correlation method on absolute values or differences between one value and the next if autocorrelation within the same variable was detected. The statistics were compiled using PAST (Hammer et al., 2001) and R software (R Core Team, 2020). Recognition of peculiar sedimentary structures and stratigraphic surfaces, and of bio- and lithofacies evolutions allowed us to evaluate

depositional depths. Thus, we defined elementary depositional sequences, almost analogous to the parasequences as re-defined by Embry (2009). Elementary depositional sequences are defined as assuming a continuous sedimentary record, accepting changes in depositional environments, and ending up with an unconformity surface.

Quadrat fossil counting was performed only on Fontblanche 1 in both sections because of its rudist abundance and diversity. The succession of the macrofossil assemblages is described, over 14.5 m (12.5 m of slick surfaces) in the Bastide d'Orves section and over 50 m (32 m of slick surfaces) in the Barre des Aiguilles section. This record was quantified by counting entire individuals as well as clasts larger than 2 cm that were identifiable with certainty. Counting was done according to 20 quadrats along the Bastide d'Orves section (A1 to A20 in Fig. 2) and to 20 quadrats also along the Barre des Aiguilles section (B1 to B20 in Fig. 3). The size of a quadrat is 0.25 m^2 (0.25 by 1 m).

Counting of the various taxa was synthesised into species richness curves. The counting data were then standardised in terms of frequencies of taxon occurrences, and dominance curves were produced from these frequencies. A dissimilarity matrix was constructed according to the Bray-Curtis dissimilarity index. A Hierarchical Ascending Classification (HAC) of the counting points was calculated from this matrix, allowing the points to be gathered into clusters supposed to represent homogeneous assemblages of taxa. The Non-Metric Multidimensional Scaling (NMDS) method was then used to visualise the distance between the reporting points using euclidean distances in a two-dimensional space, and to show the consistency of the reconstruction of the proposed biotic assemblages. The assemblage representativeness was analysed considering possible preservation biases (Tomasovych and Schlogl, 2008) and ecological and taphonomic processes (Sanders, 1999, 2001; Kidwell and Holland, 2002; Smith and Nelson, 2003; Villier, 2009).

4. Results

4.1 Litho-biofacies

4.2.1 Fontblanche 1 Unit

In both sections, the main texture of the Fontblanche 1 limestones (Figs. 4 and 5) is floatstone. However, this texture shows significant differences spanning two poles: one with a large number of bioclasts (up to 60 to 80 %; i.e., bioclast supported, as a rudstone, but within a microbioclastic-micritic matrix; ex.: Fig. 4A, B), the other with a large amount of microbioclastic-micritic matrix (up to 50 to 70 %; i.e., mud supported including bioclasts, as a packstone; e.g., Fig. 4F), or even with a wackestone texture (e.g., Fig. 5D). Textures that present microsparitic or sparitic cement are very rare and, in such cases, cement came from recrystallisation. Thereafter, texture only refers to the two rudstone and wackestone poles.

Bioclasts (Figs. 4, 5, 6), heterometric in size, come mainly from various rudists and other bivalves (*Chondrodonta*), gastropods, benthonic foraminifera and secondly from echinoderms, chaetetids, red and green algae, bryozoan, and *Bacinella/Lithocodium* (Fig. 6). Benthonic foraminifera comprise among others miliolids, *Cuneolina pavonia*, *Pseudolituonella* sp., *Charentia* sp., *Nezzazatinella picardi*, *Spirocyclina* sp., *Dictyopsella* sp., *Chrysalidina gradata*, *Hensonina tricarinata*, *Tritaxia pyramidata*, *Textularia* sp., *Ammodiscus cretaceus*, *Discorbis* sp., *Frondicularia* sp., *Rotalia mesogeensi*s (Fig. 7). In the Barre des Aiguilles section, *Praealveolina cretacea* is abundant in some beds and *Chrysalidina gradata* plus *Pseudorhapidionina* cf. *dubia* are present till the top of Fontblanche 1 (b30-32, Fig. 3). Planktonic foraminifera are scarce, poorly preserved and mainly belonging to the Hedbergellidae family. Distributions of the various taxa along both sections are given in SM 1 and 2.

The numerous whole fossils (Figs. 8, 9) in these textures appear rarely oriented as in life position, except some clusters of three to eight individuals of rudists (generally *Sauvagesia*).

However, whole rudist fossils are often well preserved, with unworn shells and their two valves sometimes still connected, so that they are regarded as parautochthonous.

The main alterations that have affected the fossils, whole or in debris, are i) dissolution and subsequent infilling of the dissolution voids, and ii) bioerosion and fragmentation.

i) Dissolution concerned specifically the inner aragonitic layer of the rudist shells (Brachert and Dullo, 2000) while the outer calcitic layer remained generally unchanged, resulting in the differential dissolution of the taxa according to their shell structure. Thus, shells comprising a thick aragonitic layer (e.g., *Caprinula*, *Ichthyosarcolites*) were partly if not totally dissolved while shells mainly composed of a cellular calcitic outer layer (e.g., Sauvagesiinae) were well preserved (except their dissolved thin aragonitic inner layer). The aragonitic shells of the gastropods *Nerinea* also were almost all dissolved. Nevertheless, the dissolution voids, particularly those from *Caprinula* and *Nerinea*, are very often filled with a lithoclastic-microbioclastic dark green (or brown if oxidised as in the Barre des Aiguilles section) sediment that includes fine quartz and glauconite grains, generally laminar and geopetal (greenish internal vadose silt). If not filled in, dissolution voids leave a clear stylolithic outline. Thus, in both cases, fossil identification was still possible, so that counting was not biased. In addition, internal cavities of Sauvagesiinae and some other taxa (particularly *Nerinea*) were frequently filled with the same laminar geopetal sediment that was infiltrated inside Fontblanche 1. Infiltration occurred from unconformities that separate elementary depositional sequences and along with early open fractures also acting as dissolution pathways (of late Cenomanian according to Floquet et al., 2013), as particularly well exposed in the Bastide d'Orves quarry (see section 4.4). When infillings of shell dissolution voids or shell cavities were incomplete, the remaining spaces were obturated with sparitic calcite. Finally, the very numerous dissolution features appear to have driven a later and complex stylolitic network (after lithostatic and tectonic stresses) so that Fontblanche 1 shows a

nodular or even brecciated-like aspect. This is particularly obvious in the Barre des Aiguilles section.

ii) Strong bioerosion/biocorrosion affected the shells, from bivalves and gastropods mainly. It consisted mostly of microborings by endolitic algae, bacteria, fungi and also of *Entobia* borings from sponges Clionidae (Figs. 4D, -F, 5A, C).

4.2.2 Fontblanche 2 Unit

Fontblanche 2 appears different in the two sections, both in lithofacies and biofacies. In the Bastide d'Orves section, Fontblanche 2 is made of 1.80 m thick limestones. Its texture is a dominantly fine bioclastic packstone (Fig. 4G), including lignite remains or carbonaceous plant debris, quartz (about 2%) and glauconite grains, framboidal pyrite. Bioclasts have been altered and come mainly from echinoderms (including crinoids ossicles), bivalves (some *Pycnodonta* debris, unrecognisable fine rudist remains), bryozoans, benthonic foraminifera (lagenids, small miliolids, *Dicyclina*, etc.). Dinoflagellate cysts (*Pithonella* cf. *ovalis*, *P.* cf. *sphaerica*) and planktonic foraminifera (particularly *Heterohelix* cf. *reussi* and *H.* cf. *globulosa*, partly pyritised) are frequent. *Whiteinella* cf. *archaeocretacea* is present. These facies were bioturbated and present a nodular aspect. They are topped with a discontinuity (firmground, D_{BO} in Fig. 2) that is overlain by the clayed limestones of the nodosoides ammonite zone (NBNL in Fig. 2).

In the Barre des Aiguilles section, Fontblanche 2 is 12-13 m thick and constitutes the upper part of the ancient quarry which was not exploited by cable sawing. It appears to be made of coarse facies, essentially rudistid packstones to floatstones with some quartz grains (Fig. 5E, microsample b35), as in its type-locality of Fontblanche (FB in Fig. 1C) (Crumière-Airaud, 1991; Philip, 1998; Floquet et al., 2018). These facies include entire to almost entire shells or large remains from rudists or heterometric bioclasts within an almost microbioclastic matrix (average size: 20 μm; rarely micritic). Rudists seem to be represented essentially by

Sauvagesiinae and particularly by the genus *Durania* (among which *Durania* cf. *arnaudi*), some of them in clusters of six to eight individuals still in life position (Fig. 3, elevation 42 m). According to Philip (1978), scarce Radiolitinae [cf. *Radiolites lusitanicus*, *R. peroni* (a synonym of *R. lusitanicus*), *R.* aff. *praesauvasegi*] could be encountered. Sauvagesiinae opercular left valves are sometimes found together, isolated from their right valves. Rudist shells remains or bioclasts are always angular, fragmented and not rounded, and sometimes biocorroded or micritised (microsamples b33 to b39 in Fig. 3). There are almost no other identifiable bioclasts than those from rudists except some micritised benthonic foraminifera, often transformed into peloids (Fig. 5E).

Fontblanche 2 ends up with a sharp erosive surface (D_{BA} in Fig. 3) disconformably overlain by quartzose limestones (Fig. 5F) which correspond to the 'A4 Unit' *sensu* Hennuy, 2003 or to the 'Dent de Chat Quartzose Calcarenite Formation' *sensu* Floquet et al. (2018), of early Coniacian age (Fig. 3). Quartz grains infiltrate in the upper part of Fontblanche 2 thanks to burrows which start from the final surface.

4.2 Fontblanche 1 biotic assemblages

The Fontblanche 1 macroscopic fossil record from the Bastide d'Orves and Barre des Aiguilles sections (Figs. 8 and 9) is characterised by the occurrence of 12 taxa, seven of which being rudists: *Sauvagesia sharpei* Bayle 1857 (Radiolitidae), *Durania arnaudi* Choffat 1891 (Radiolitidae), *Apricardia* sp. (Requienidae), *Ichthyosarcolites bicarinatus* Gemmellaro 1865 (Ichthyosarcolitidae), *Caprinula boissyi* d'Orbigny 1840 (Caprinulidae), *Caprotina* sp. (Caprotinidae), *Caprina* sp. (Caprinidae), *Chondrodonta joannae* Choffat 1886 (Chondrodontidae), *Nerinea* sp. (Nerineidae), Chaetetidae (Porifera), Scleractinia (Anthozoa), Cidaroida (Echinoidea). The genus *Caprina* is very rare, unlike *Caprinula*, and has never been counted inside the quadrats. No Monopleuridae were identified in either locality, but a relict presence is mentioned by Philip (1978). The two taxa *Sauvagesia sharpei* and *Durania*

arnaudi are sometimes easily identifiable from to the presence or absence of ligamentary crest when the body cavity outline is entirely visible but they are often found as clasts and therefore not identified at a specific level. Thus, reference will be made only to their subfamily Sauvagesiinae for the quantitative study.

Taxa frequencies (Figs. 10, 11; SM 3) were obtained from the counting within quadrats. The HAC (Fig. 12) identifies four clusters of counting points with comparable taxon assemblages. The NMDS method displays the 40 counting points in these four clusters (Fig. 13). Thereafter, we assumed that the clusters correspond to the four biotic assemblages, namely the *Chondrodonta* assemblage (A), the *Apricardia*-Sauvagesiinae assemblage (B), the *Caprotina* assemblage (C), and the *Nerinea* assemblage (D) (Figs. 12, 13). (A) The *Chondrodonta* assemblage (Fig. 13A) includes 13 counting points and is the most heterogeneous. The characteristic taxon of this assemblage is *Chondrodonta joannae*, ranging from 95.8 % (B2) to 11.4 % (B9). Points with a maximal abundance of *Chondrodonta*, specifically in the Barre des Aiguilles section, correspond to the accumulation of horizontally arranged shells. *Chondrodonta* can be associated with rudists, generally Sauvagesiinae (maximum: B15, 51.4 %), and also *Ichthyosarcolites* (maximum: B5, 32.1 %) and *Caprotina* sp. (maximum: B9, 23.7 %). *Caprinula* and Chaetetidae are present occasionally. (B) The *Apricardia*-Sauvagesiinae assemblage (Fig. 13B) includes 22 counting points and is the most common. This assemblage is much more homogeneous than the *Chondrodonta* one, with *Apricardia* and Sauvagesiinae largely dominant on all points (minimum: A4, 72.7 %; maximum: B19 and B20, about 100 %). Two poles appear well-illustrated by the NMDS: one dominated by *Apricardia* (B16, *Apricardia*: 90.4 %, Sauvagesiinae: 1.2 %) and one dominated by Sauvagesiinae (A3, *Apricardia*: 0 %, Sauvagesiinae: 87 %). Furthermore, a Fischer's exact test supports the hypothesis that *Apricardia* and Cidaroida are mutually exclusive (p-value: 0.02). Cidaroids are mostly identified by isolated plates and spines

probably scattered after their death by currents. However, the negative correlation is an evidence that the cidaroids are at least parautochthonous (it would be very unlikely to obtain a significant correlation if frequencies of cidaroids were driven by currents). Concerning *Apricardia*, the two *Apricardia* and Sauvagesiinae poles cannot be separated into two distinct assemblages, as no clear boundary can be assigned (Fig. 12). *Chondrodonta* is occasionally present as well as *Caprinula* but the latter only when Sauvagesiinae are dominant. (C) The *Caprotina* assemblage (Fig. 13C) is represented only by three points. *Caprotina* is the dominant taxon (minimum: B3, 31.4 %; maximum: B12, 78 %). *Ichthyosarcolites* is also found in two of the three points (B12, 1.5 %; B3, 33.6 %) and *Nerinea* in point B3 (29.5 %), resulting in a high heterogeneity of the faunal composition of this assemblage. (D) The *Nerinea* assemblage (Fig. 13D) is represented by two points where this taxon is largely predominant (B14: 58.7 %; B13: 90.1 %). This high abundance appears only once, in the Barre des Aiguilles, with shells axis randomly oriented in the stratification plane. *Chondrodonta* can be associated with relative abundance (B14: 21.4 %).

4.3 Species richness and bioclastic fraction

The Pearson correlation coefficient does not reveal a significant correlation between the species richness and the bioclastic fraction in the Bastide d'Orves and Barre des Aiguilles sections taken together. However, a positive correlation can be reported throughout the Bastide d'Orves section alone (within Fontblanche 1, correlation coefficient: 0.36; p-value: 0.04). In the Barre des Aiguilles section alone, there is also a significant correlation between the species richness and the bioclastic fraction, specifically within Fontblanche 1 (microsamples b1 to b32 in Fig. 3; correlation coefficient: 0.49; p-value: 0.02).

Then, within Fontblanche 2 (from microsample b33 up to b39 in Fig. 3), the species richness decreases while the bioclastic fraction increases, but without any significant correlation (correlation coefficient: -0.51; p-value: 0.13). Finally, an ANOVA test is used to show if there

are differences in bioclastic fraction between the four biotic assemblages defined above. The analysis shows that the assemblages explain only a small part of the variation in the bioclastic fraction (average of the square deviations: 76.05 for the part explained by the assemblages, 249.39 for the part not explained by the assemblages).

4.4 Fontblanche 1 elementary depositional sequences and succession of biotic assemblages

Within Fontblanche 1, in both sections, the presence of obvious sedimentological unconformities (SM 4 to 6) plus changes of lithofacies and biotic assemblages allow us to recognise elementary depositional sequences. Six sequences are recognised in the Bastide d'Orves section ($S_{BO}1$ to $S_{BO}6$ in Fig. 2) and five in the Barre des Aiguilles section ($S_{BA}1$ to $S_{BA}5$ in Fig. 3). We postulate that such sequences record variations of accommodation (see Guillocheau, 1995). The created accommodation spaces could be filled differently and at different rates according to the carbonate fabrics (Masse and Montaggioni, 2001). Variations of neritic carbonate production-accumulation modify directly the positive accommodation versus sedimentary supply ratio, and thus influence the increases or decreases of palaeodepths and bed thicknesses. At the extreme, we could expect, in the hypothesis of a constant positive accommodation, that variations of carbonate production-accumulation could control per se the development of elementary depositional sequences (Dalmasso and Floquet, 2001). Finally, sequences and unconformities of both sections, except the final Fontblanche 1 unconformity ($D_{BO}6$ in Fig. 2 and $D_{BA}5$ in Fig. 3), cannot be correlated.

4.4.1 Bastide d'Orves section

Sequence $S_{BO}1$. The texture is packstone-floatstone comprising many highly heterometric bioclasts in a micritic-microbioclastic matrix (Fig. 4A). $S_{BO}1$ shows a single parautochthonous *Apricardia*-Sauvagesiinae assemblage ($S_{BO}1a$ in Fig. 2) where Sauvagesiinae dominate (average A1-2: 77.2 %) over *Apricardia* (average A1-2: 13.3 %).

A strong reworking of the bioclastic packstone ends $S_{BO}1$. Coarse floatstone-rudstone with numerous blackened shells remains are elements of the unconformity $D_{BO}1$ (SM 4A). The rudstone infiltrates down inside $S_{BO}1$. A new biotic assemblage including more *Caprinula* (C in SM 4A) appears above this reworking bed.

Sequence $S_{BO}2$. The texture is mainly floatstone with many heterometric and angular bioclasts, some of them joined, in a microbioclastic to micritic matrix (Fig. 4B). The percentage of bioclasts tends to decrease upwards. $S_{BO}2$, as a whole, yields the *Apricardia*-Sauvagesiinae assemblage while in detail it exhibits three successive assemblages ($S_{BO}2a$, $S_{BO}2b$ and $S_{BO}2c$ in Fig. 2). In $S_{BO}2a$, Sauvagesiinae initially dominate widely without *Apricardia*. *Caprinula* shells are also present, in low proportions (A3: 11.4 %). In $S_{BO}2b$, the occurrence of *Caprinula* increases (A4: 20.35 %) together with numerous *Apricardia* (A4: 37.6 %) at the expense of Sauvagesiinae (A4: 35.01 %). Then the percentage of Sauvagesiinae-*Apricardia* remains similar while the percentage of *Caprinula* decreases sharply (A5: 2.7 %) and that of *Chondrodonta* increases (A5: 13.4 %). In $S_{BO}2c$, the percentage of *Apricardia* decreases (A6: 12.7 %), leading to an assemblage largely dominated by Sauvagesiinae (A6: 83.3 %), as in $S_{BO}1$. *Ichthyosarcolites* appears very rare in $S_{BO}2$.

$S_{BO}2$ ends with a finely bioclastic yellowish wackestone partly reworked and exhibiting irregular vertical spaces deeply infilled by a greenish floatstone which constitutes the base of $S_{BO}3$ (SM 5A). In addition, this wackestone presents open burrows, fine root traces, borings, and fenestrae laterally. All these features characterise the unconformity $D_{BO}2$.

Sequence $S_{BO}3$. The overall texture is floatstone, as for $S_{BO}1$ and $S_{BO}2$, including almost entire rudists and heterometric bioclasts within a generally microbioclastic matrix but, in some places, within a micritic matrix so that the texture is packstone (Fig. 4C). Rare glauconite grains are found at the base. $S_{BO}3$ contains the *Apricardia*-Sauvagesiinae assemblage but the

ratio of the two taxa evolves so that three assemblages are distinguished (S_{BO}3a, S_{BO}3b and S_{BO}3c in Fig. 2). Sauvagesiinae dominate largely in this sequence.

The unconformity D_{BO}3 consists of a truncation and a reworking of the top of S_{BO}3 from which a network of dissolution cavities develops. The cavities are subsequently filled in firstly by a finely bioclastic and micritic sediment, and secondly by a dark green (brown if oxidised) finely bioclastic and lithoclastic sediment (SM 4B). Lithoclasts are made of S_{BO}3 facies, formerly indurated, particularly from the walls of the dissolution cavities (SM 4C-D). The second infilling sediment includes glauconite and quartz grains, framboidal pyrite, and rare planktonic foraminifera. It infiltrates also within the rudists internal cavities (SM 4B) as well as in the voids corresponding to the dissolution of the inner aragonitic layer of rudists shells, notably those of *Caprinula* (SM 4D).

Sequence S_{BO}4. It is marked by a very high dominance of *Chondrodonta* (average 83 %, A12-14) within a floatstone to packstone texture (microbioclastic to micritic matrix, Fig. 4D, microsample a19) which includes locally numerous peloids. *Chondrodonta* does not present a peculiar orientation.

The unconformity D_{BO}4 consists, exactly as D_{BO}3, in truncation and reworking (SM 5B). Thus, the top of S_{BO}4, which appears to have been previously indurated (borings are still recognisable), is eroded, and part of its rudistid content is reworked inside the base of S_{BO}5 (as evidenced by differences in colours, SM 5B). Meanwhile, facies of the base of S_{BO}5 infiltrate down in dissolution voids of S_{BO}4.

Sequence S_{BO}5. The main texture remains floatstone-packstone rich in peloids (Fig. 4E, microsample a23), rarely wackestone, in which the *Apricardia*-Sauvagesiinae assemblage dominates. The unconformity D_{BO}5 that ends S_{BO}5 has the same characteristics as D_{BO}4.

Sequence $S_{BO}6$. The same floatstone to packstone texture predominates with locally a micritic matrix and thus a packstone-wackestone texture (Fig. 4F, microsample a27). $S_{BO}6$ yields two successive *Apricardia*-Sauvagesiinae assemblages ($S_{BO}6a$ and $S_{BO}6b$ in Fig. 2).

$D_{BO}6$ at the top of both $S_{BO}6$ and Fontblanche 1, directly covered by the drastically different Fontblanche 2 Unit (SM 5C), shows similar characteristics to those of the underlying unconformities: truncation-erosion, dissolution, and infilling of the resulting voids by sediments of the overlying unit. Large cavities, irregular in shape, as well as open fractures, develop deeply below the unconformity down to the lower depositional sequences. This network is filled in with a dark green (brown if oxidised) finely bioclastic and lithoclastic sediment (SM 4B). Lithoclasts are made of formerly indurated $S_{BO}6$ facies, particularly from the walls of the dissolution cavities (SM 4C-D). In addition, this sediment includes glauconite and quartz grains, framboidal pyrite, and rare planktonic foraminifera. The top surface is a hardground as evidenced by borings, iron oxide crust (SM 6A) as well as oyster encrustation. The radical facies change between Fontblanche 1 and Fontblanche 2, is highlighted by the fine packstone rich in dark glauconite grains just over $D_{BO}6$ (SM 6A). This unconformity is of regional extension (Floquet et al., 2018; Floquet, 2020).

4.4.2 Barre des Aiguilles section

Sequence $S_{BA}1$. The overall texture along the 24 m thickness is floatstone to packstone comprising numerous heterometric bioclasts in a microbioclastic to micritic matrix. The biota is very rich and diverse in terms of taxa (Fig. 11). We defined here seven successive assemblage sub-sequences ($S_{BA}1a$ to $S_{BA}1g$ in Fig. 3) related to taxonomic composition changes. $S_{BA}1a$ is made of a thin bed, laterally continuous over 50 m with dominant *Caprotina* (70.5 %) still in life position in bouquets, plus *Ichthyosarcolites* (24.4 %) and Nerineidae (4.7 %) (B1 in Fig. 3). $S_{BA}1b$, 30 cm thick, is largely dominated by *Chondrodonta* (95.8 %, B2) whose shells are arranged in the stratification plane. $S_{BA}1c$, 2 m thick, is made

of an assemblage of Nerineidae (29.5 %), *Caprotina* (31.4 %), *Ichthyosarcolites* (33.6 %) and Sauvagesiinae (3.5 %) (B3). The first three assemblages S_{BA}1a-c comprise also diversified benthonic foraminifera (Fig. 9). S_{BA}1d, 13 m thick, is composed of *Chondrodonta* (average 35.5 %, B5 to B11), *Apricardia* (average 30.6 %), *Ichthyosarcolites* (average 16.7 %) and *Caprotina* (average 10.7 %) plus rare Chaetetidae, corals and cidaroids. S_{BA}1e is composed of dominant parautochthonous *Caprotina* (78 %, B12), *Chondrodonta* (11.4 %), Sauvagesiinae (6.8 %), rare *Ichthyosarcolites* (1.52 %; this rudist disappearing thereafter in the section), accompanied by abundant *Praealveolina cretacea*, within a packstone-floatstone texture (Fig. 5A, microsample b14). S_{BA}1f is characterised by the abundance of Nerineidae (from 90.1 % in B13 down to 58.6 % in B14), their shell axis randomly oriented in the plane of stratification, plus *Chondrodonta* (from 5.9 % up to 21.4 %), *Apricardia* (maximum of 10 % in B14), Sauvagesiinae (from 1.2 % to 8.1 %). *Caprotina* disappears in B14. S_{BA}1g includes quite equally Sauvagesiinae (51.4%) and *Chondrodonta* (48.6%).

S_{BA}1 ends with an irregular lithoclastic bed made of black and beige pebbles (SM 6B), mixed with rudist debris, indicating erosion and reworking. The matrix is composed of fine lithoclasts, numerous carbonate glaebules or peloids (*sensu* Freytet and Plaziat,1982; Wright, 1994), and includes quartz grains. This matrix infiltrates down inside S_{BA}1 in prior dissolution voids. Such a conglomeratic bed characterises the unconformity D_{BA}1. In addition, above D_{BA}1, a net change of biotic assemblage occurs (between B15 and B16 in Fig. 11).

Sequence S_{BA}2. It shows two assemblages S_{BA}2a and S_{BA}2b (Fig. 3). S_{BA}2a, 1 m thick, is made of a *Chondrodonta* assemblage accompanied by Sauvagesiinae, in a floatstone texture. S_{BA}2b, 4 m thick, is made of the first *Apricardia*-Sauvagesiinae assemblage of the section, with *Apricardia* largely dominant (90.4 %, Fig. 11, B16) plus Nerineidae (5.2 %), *Chondrodonta* (2 %), Sauvagesiinae (less than 2 %) and *Caprotina* (0.8 %), in a packstone-floatstone texture with a dominant micritic matrix including heterometric and highly

20

micritised bioclasts, especially the numerous benthonic foraminifera (Fig. 9) transformed into peloids (Fig. 5B, microsample b24). *Caprotina* disappears from $S_{BA}2$ in the rest of the section.

The unconformity $D_{BA}2$ corresponds to a truncation of the benthonic foraminifera rich wackestone at the top of $S_{BA}2$. It is topped by the $S_{BA}3$ floatstone composed of an *Apricardia*-Sauvagesiinae community.

Sequence $S_{BA}3$. About 2 m thick, it is composed of a single *Apricardia*-Sauvagesiinae assemblage with dominant *Apricardia* (average 65.5 %, B17-18) and subordinate Sauvagesiinae (average 30.2 %) plus *Chondrodonta* (5.3 %, B18), in a packstone to floatstone texture (Fig. 5C, microsample b27). The species richness is high (11 taxa) and the bioclastic fraction low (15%; Fig. 3).

The unconformity $D_{BA}3$ corresponds also to a truncation of the top of $S_{BA}3$ made of a wackestone-mudstone texture comprising micritic nodules delimitated by circum-granular cracks. The truncation is accompanied by a thin and irregular reworking bed that includes these nodules in form of black pebbles. A floatstone composed of numerous *Apricardia* shells directly overlies this reworking bed.

Sequence $S_{BA}4$. The sequence is about 1.80 m thick and is characterised by a new *Apricardia*-Sauvagesiinae assemblage, but almost monospecific with 96.6 % *Apricardia* (average B19-20, Fig. 3) in a packstone to wackestone texture owing to an abundant micritic matrix (Fig. 5D, microsample b28).

$S_{BA}4$ ends with the unconformity $D_{BA}4$ which exhibits almost all the same features as those of $D_{BA}3$.

Sequence $S_{BA}5$. The sequence holds two assemblages: $S_{BA}5a$ and $S_{BA}5b$ (Fig. 3). $S_{BA}5a$, less than 1 m thick, includes many *Chondrodonta*. $S_{BA}5b$, about 1.30 m thick, comprises an

Apricardia-Sauvagesiinae assemblage with a dominance of Sauvagesiinae. Textures are bioclastic packstones to wackestones due to a dominantly micritic matrix which contains numerous benthonic foraminifera (Fig. 9), particularly *Chrysalidina gradata* (microsamples b30, 31, 32 in Figs. 3, 9) and *Pseudorhapidionina* cf. *dubia* (microsample b32). The species richness is high while the bioclastic fraction in the matrix is low (Fig. 3).

The ultimate unconformity $D_{BA}5$, is a truncation of the around 0.6 m upper $S_{BA}5b$ micritic limestones which present a dense network of cavities, notably from the dissolution of rudists and gastropods shells, and from burrows and fractures (SM 6C). The micritic matrix is structured in peloids and peloidal nodules defined by circum-granular cracks. The cavities are filled with geopetal peloidal micrite or with a fine bioclastic and lithoclastic sediment including corroded quartz (grain size range from 100 up to 600 μm). This sediment is amber-coloured by an oxidised organic matter of plant origin (SM 6C). A bioclastic packstone including quartz, typical of the Fontblanche 2 Unit, directly overlies the truncation (boundary within microsample b32 in Fig. 3). Bioclasts are essentially from radiolitid rudists so that a drastic drop in biodiversity accompanies the $D_{BA}5$ unconformity (Fig. 3).

5. Interpretations and discussion

5.1 Depositional environments

5.1.1 Fontblanche 1 overall depositional environment

The fossil assemblages from both Bastide d'Orves and Barre des Aiguilles sections, especially the rudists, the very abundant benthic foraminifera, the red and green algae (the dasycladale *Acicularia* notably), indicate that the Fontblanche 1 overall depositional palaeoenvironment was a tropical shallow marine carbonate platform (the South-Provence Basin was located around 30° N during the late Cenomanian, Fig. 1B). In addition, the dominant micritic and microbioclastic matrix of the limestones, the absence of rounded bioclasts or other grains due to hydrodynamic processes and, on the contrary, the heterometric fragmentation of the

bioclasts as a result of intense biocorrosion, prove a quiet environment: an inner and sheltered position within the carbonate platform. The activity of microborers led to the creation of micrite envelopes around the shells (Fig. 5B) and, when intensive, such biocorrosion could lead to the complete replacement of the skeletal grains by micrite (Bathurst, 1966) and hence generating part of the matrix. Otherwise, the activity of microborers has caused severe fragmentation of the shells, in particular of the fragile cellular calcitic outer shell of the Sauvagesiinae, producing microbioclasts (Amico, 1977) that constitute the other part of the matrix. From this point of view, bioclasts and microbioclasts, if not biocorroded, appear almost always angular (e.g., Fig. 4A, B, C, D) and not rounded by hydrodynamic processes. A possible explanation of the fragmentation of shells into angular bioclasts before micritisation could be the predation by durophagous vertebrates (Martill et al., 1994; Citton et al., 2019). Some benthonic foraminifera were also micritised and transformed into peloids (e.g., Fig. 5A, B). To summarise, the bulk of sediment production was due to shell or test bioerosion and biofragmentation, mainly from rudist shells, producing loose detritus that consisted of poorly sorted skeletal debris and a silty-muddy matrix.

5.1.2 Fontblanche 1 subaerially exposed elementary depositional sequences

The unconformities that cap the elementary depositional sequences clearly express emersions: i) the blackening of the shells associated with the $D_{BO}1$ unconformity (SM 4A) probably resulted from adsorption of organic matter under suboxic or anoxic conditions, as such a phenomenon occurs in a mediolittoral setting (Bernier and Strasser, 1988); ii) the rootlet traces, open burrows, and fenestral fabric of the $D_{BO}2$ unconformity (SM 5A) indicate a supratidal setting and long-lasting emersion; iii) the numerous dissolution features well recognisable in almost all unconformities (e.g., $D_{BO}3$, $D_{BO}4$, $D_{BO}6$ in SM 4B, C, D, 5C, D, 6A and $D_{BA}5$ in SM 6C) are representative of palaeokarst; iv) the black pebbles, associated with the $D_{BA}1$ (SM 6B), $D_{BA}3$ an $D_{BA}4$ unconformities in the Barre des Aiguilles section, are

regarded as results of staining by a terrestrial organic matter of limestones or pedogenic calcretes reworked from peritidal and palustrine carbonate environments, according to Strasser and Davaud (1983), Wright and Tucker (1991), Wright (1994).

The unconformities express also net marine transgressions that succeeded the emersion episodes and initiated new elementary depositional sequences. Each unconformity exhibits truncation and reworking (SM 3, 4, 5) that characterise a basal flooding surface. Reworking concerned simultaneously materials of both terrestrial (quartz, plant remains, pedogenic nodules) and marine (glauconite, foraminifera, bioclasts) origins, which were trapped and preserved in the various cavities (from dissolution, burrows, open fractures; e.g., SM 4B, C, D). Consequently, each Fontblanche 1 elementary sequence resulted from a basal flooding-deepening and then from a shallowing upward, so that these sequences appear similar to the 'punctuated aggradational cycles' *sensu* Goodwin and Anderson (1985). The flooding allowed the settlement and development of the successive rudist and commensal organisms communities whose biogenic carbonate production-accumulation led to the progressive fill-in of the created space for sedimentation till emersion.

However, accurately determining the maximum depositional palaeodepth within a sequence is still a challenge. In a general way, the palaeodepths within the inner carbonate platform ranged between zero (intertidal to supratidal) and few metres (subtidal). Assuming that the created spaces for sedimentation (deepening) were maximum at the base of the sequences and taking into consideration the sediment compaction, the thinnest sequences (about 2 m thick as $S_{BO}2$ or $S_{BO}5$) could have formed in three to four metres depth at the most. Moreover, if positive accommodation and carbonate production/accumulation were almost in balance during the development of the sequences, resulting thicknesses could be largely greater than the value of the reached maximum palaeodepth of a very few metres (Dalmasso and Floquet, 2001).

5.1.3 Fontblanche 2 depositional environments

In the Bastide d'Orves section, a radical change of depositional environment occurred above the Fontblanche 1 $D_{BO}6$ final unconformity that resulted from net emersion and erosion (Fig. 2, SM4C, SM5A). The Fontblanche 2 fine bioclastic texture, glauconite content, renewed biota made of echinoderms, bivalves, bryozoans, benthonic foraminifera (lagenids), planktonic foraminifera (with numerous *Heterohelix*), dinoflagellate cysts (*Pithonella*) indicate a marine transgression coupled with a marked deepening. Thus, environments became infralittoral to circalittoral and opened southwards to the basin *s.s.* (green in Fig. 1C). Consequently, almost all rudist and commensal communities of the previous inner shallow carbonate platform disappeared.

In the Barre des Aiguilles section, an environmental change is also recorded in the Fontblanche 2 lithobiofacies above the $D_{BA}5$ unconformity tied to emersion and erosion (Fig. 3, SM 6C). Rudists are present, but in oligospecific to monospecific assemblages mainly composed of *Durania* plus some *Radiolites*. The packstone to floatstone textures, the presence of bryozoan, echinoderms, *Bacinella* nodules, planktonic *Pithonella* and *Heterohelix* indicate a new infralittoral environment unpropitious for the settlement of diversified rudistid communities as in Fontblanche 1, and in which bioclastic sands mainly were spread out. This change was homologous to the one recorded in the Fontblanche type-locality (Fig. 1) (Crumière-Airaud, 1991). It seems to have been associated with a slight deepening and also with an opening to the basin. From this point of view, *Bacinella* is generally encountered from subtidal shallow waters of open marine environments (Rameil et al., 2010).

5.2 Time-averaging, biocorrosion and their negative effect on biodiversity sampling

Biocorrosion of the rudist shells, meant to occur during the bivalve's lifetime as well as just after their death (Flügel, 2010), was the main factor of bioclast production (Sanders, 1999). The positive correlation between the bioclastic fraction and the species richness in both

Bastide d'Orves and Barre des Aiguilles Fontblanche 1 sections (Figs. 2, 3) is regarded as an accurate evidence of the effect of biocorrosion on perceived species richness. The greater the corrosion, the more difficult it becomes to identify taxa precisely, which artificially decreases the species richness. A taphonomic continuum exists between the whole rudist shells, then perforated, broken and biocorroded, generating smaller and smaller bioclasts and finally a micrite binding the remaining shells and bioclasts. The microbioclastic to micritic matrix appears to be the ultimate result of biocorrosion. The bioclasts/matrix fraction therefore reflects the intensity of shell degradation. Significant biodegradation thus leads to a decrease in biodiversity. This is particularly the case of the benthonic foraminifera that are very often micritised. When species richness and bioclastic fraction are correlated, the decrease in biodiversity is therefore an artefact and reflects the taphonomic conditions of the sedimentary environment.

Within Fontblanche 2, there is no longer a significant correlation between species richness and bioclastic fraction, which is especially well expressed in the Barre des Aiguilles section (Fig. 3, above sample b32). The loss of biodiversity here reflects an ecological reality that is independent of taphonomic processes. Only an oligospecific rudists community survived the opening and deepening, and almost all the benthic microfauna disappeared (Fig. 9).

A relationship between an increase in bioclastic fraction and the gain of taxonomic richness may reflect a combination of taphonomic and ecological triggers. Large and robust shells decay progressively in coarse, irregular grains through biocorrosion processes (biofragmentation). After a limited time of degradation, only large bioclasts are produced. Only a longer lasting time allows grains to be transformed into micrite. More shells are highly altered in fine-grain sediments and smaller shells are likely to disappear selectively with increasing alteration (e.g., Martin, 1999). In such a sedimentary environment with limited mixing, as time goes by, the quantity of mud increases and the quantity of well-preserved

shells decreases. A lower content of bioclastic sand and a higher mud content modify the seafloor properties and sand dwellers become rarer in favour of mud dwellers. The lower the mean sedimentation rate is, the higher the time-averaging is, and higher is the intensity of biocorrosion. Under these conditions, the quality of the fossil record becomes less and less good, which affects our perception of biodiversity.

5.3 Ecotypes, rudist communities and ecosystems

The ecology of rudists taxa can be linked to a mode of nutrition related to the position of the commissure in relation to the substratum (Skelton, 1978, 1991; Gili and Skelton, 2000; Gili and Götz, 2018). Position and orientation of the commissure is itself dependent on the stability of the substratum. Three main rudist ecotypes are distinguished (Skelton, 1978, 1991): (i) elevators, which were adapted to substrates with positive sediment accumulation, and which could develop into densely packed groups of individuals; (ii) recumbents lying down on the sediment which had a large area in contact with the substrate that allowed them to stay steady in unstable environments where sediment bypassing was more important than sediment accumulation; (iii) clingers, which formed an intermediary between recumbents and elevators, slightly buried obliquely in a stable firm substrate with a few sediment accumulation. From the elevators, a fourth ecotype of encrusters can be defined, which keep living on a hard substrate throughout their development. Consequently, the nature and rate of sediment production due to the development of rudist communities and to the degree of degradation of their shells resulting in different substrates may have exerted feedback control on the rudist ecotypes (Steuber and Löser, 2000). This or that ecotype might have been favoured by a highly bioclastic substrate, i.e., grainy and firm, or by a microbioclastic-micritic one, i.e., silty-muddy and soft. All rudist shells are parautochthonous *sensu* Kidwell and Holland (1991), allowing to discuss community-environment interactions. However, not all *Chondrodonta* and *Nerinea* shells from the *Chondrodonta* and *Nerinea* communities appear

to have been preserved in situ. The numerous *Chondrodonta* shells in $S_{BA}1b$ (Figs. 3, 11) with their two valves still connected and all arranged parallel to the bedding (Fig. 13A) are regarded as allochthonous and accumulated after an event of high hydrodynamics (tempestite *sensu* Ayoub-Hannaa and Fürsich, 2011). The unique *Nerinea* assemblage in $S_{BA}1f$ (Fig. 3) with the shell axis randomly oriented in the stratification plane probably resulted too from the action of storms and cannot be interpreted as a biotic community. Finally, the three biotic communities that can be extrapolated from the three '*Caprotina*', '*Chondrodonta*', and '*Apricardia*-Sauvagesiinae' assemblages did not develop solely based on the bioclastic content and substrate differences, but also on biological interactions within ecosystems through time.

In unsettled environments with soft muddy to silty substratum, in conjunction with harsh environmental conditions, the *Caprotina* community was the first to develop in the studied locations. This community is predominantly composed of *Caprotina* and accompanied by *Ichthyosarcolites. Ichthyosarcolites* are known to have been pioneers of soft and unstable substrates such as mudflats, where the environmental parameters prevented the survival of other rudists: clayed sedimentation, high hydrodynamism, low lighting (Chéreau et al., 1997; Videt, 2003). *Ichthyosarcolites* were large organisms (diameter up to 1 m) whose shells may have been used as a stable and hard substrate by commensal taxa. Thus, the encrusting taxa *Caprotina* upon *Ichthyosarcolites* shells formed a characteristic association whose dominance in the lower part of Fontblanche 1 in the Barre des Aiguilles section ($S_{BA}1a$, $S_{BA}1c$, $S_{BA}1e$) triggered the invasion of the carbonate platform by rudists, forming a pioneering commensal association.

Ichthyosarcolites are continuously present from the base up to more than 20 m in the Barre des Aiguilles section. They persisted in the South-Provence carbonate platform long after its colonisation, in *Chondrodonta* communities, as also occurred in the Aquitanian Basin

(western France) (Chéreau et al., 1997). This persistence was concomitant with the development of populations of Sauvagesiinae and *Chondrodonta*, two 'mud-sticker' bivalves (Seilacher, 1984) which both played a role in the stabilisation of the substrate (Ayoub-Hannaa and Fürsich, 2011; Posenato et al., 2020). They pursue the stabilisation of the environment begun by *Ichthyosarcolites*. *Caprotina* blooms regularly intersperse within *Chondrodonta* communities, where they formed thin monospecific sheets in bouquets covering the entire substratum by a single generation. *Chondrodonta* is the only other bivalve found with the rudists on the two sections. In the Cenomanian, several genera of oysters can be very abundant in shallow water environments (*Rhynchostreon*, *Ceratostreon*, *Rastellum*, *Hyotissa*, *Pycnodonta*), but in the South-Provence Basin and elsewhere in the world, an ecological exclusion seems to prevent the development of populations other than *Chondrodonta* in areas where rudists proliferate (Janson et al., 2015; Gili et al., 2016; Posenato et al., 2020). This exclusion is explained by the fact that the development of constratal rudists with a commissure a few centimetres above the sediment on carbonate platforms in dense congregations prevents the appearance of oysters due to spatial competition. *Chondrodonta* on the other hand have a superstratal lifestyle due to their particular morphology; these can rise 10 to 20 cm above the sediment. This factor, together with environmental instability before the Oceanic Anoxic Event 2, particularly of cooling phases, may have played a role in favour of r-strategy opportunists such as chondrodonts (Posenato et al., 2020). This last hypothesis may partially explain why in *Chondrodonta* communities, Sauvagesiinae never become dominant.

When the environment is stabilised by the joint action of *Ichthyosarcolites*, *Chondrodonta*, and Sauvagesiinae, Sauvagesiinae expands, leading to the settlement of an *Apricardia*-Sauvagesiinae community. This transition is corroborated by the closeness of the *Chondrodonta* and *Apricardia*-Sauvagesiinae communities in terms of taxonomic content

(Fig. 12). The *Apricardia*-Sauvagesiinae community is composed of *Apricardia* as clinger, and *Sauvagesia sharpei* and *Durania arnaudi* as elevators. It is constituted of a continuum between two dominant poles, one with Sauvagesiinae, one with *Apricardia* (Fig. 12) that could be partially related to two different, although close, ecotypes in a continuum of carbonate production having in common a relatively stable environment with probable fluctuations in water depth and sedimentation rate. The Sauvagesiinae dominant pole could have corresponded to a high sedimentation rate (and a rather bioclastic firm substrate) in a depth of one to a few metres, whereas the *Apricardia* dominant pole could have conformed with a weak sedimentation rate (and a rather microbioclastic to micritic soft substrate) in a reduced depth (may be about one metre or less according to Floquet, 1991 and Masse et al., 2003). This is corroborated by the negative relationship between the presence of *Apricardia* and Cidaroida. When the environment became more restricted, *Apricardia* developed and Cidaroida disappeared because of their low tolerance to salinity variations. The commensal rudist *Caprinula* can be found in this assemblage but the *Apricardia* domination of the substrate seems to have controlled the *Caprinula* populations by restricting their development (Figs. 8, 12).

From a broader perspective, the high abundance of Sauvagesiinae in the two sections studied was coeval with the ecological success of this subfamily in relation to the beginning of the upper Cretaceous radiation of the Radiolitidae (Skelton, 2003; Steüber et al., 2016; Rineau, 2017; Rineau et al., 2020). At this time, dense congregations of elevators such as the Radiolitidae conquered new ecosystems by colonising spaces where other rudists (and corals) could not live anymore. In these places, Radiolitidae grow in important monospecific biostromes and become the dominant rudist family in carbonate platforms. Ten Radiolitidae genera are extant during the Cenomanian, from which six appear during this stage (*Distefanella, Praeradiolites, Radiolites, Sphaerulites, Neoradiolites, Polsakia*).

Sauvagesiinae and *Durania* appear before, during the Aptian and Albian, respectively, and represent the radiation onset of Radiolitidae. The Cenomanian/Turonian boundary is also the place of an important extinction for rudists, due to the Oceanic Anoxic Event 2 were canaliculated rudists disappear entirely from the fossil record for almost 8 Myr. *Caprotina*, *Ichthyosarcolites*, and *Caprinula* disappear during this event. Upper Cenomanian rudist communities of the South-Provence Basin reflect this unique transition phase in the evolution of rudists, with the radiation of Radiolitidae and canaliculated rudists, and the disappearance of Ichthyosarcolitidae, Caprotinidae, and most canaliculated rudists thereafter (Philip and Airaud-Crumière, 1991; Rineau, 2017; Rineau et al., 2020). During this time, rudist diversity reaches a peak (Steuber et al., 2016), and complex ecological successions arose. The two sections studied here reflect this deep ecosystemic change which was evidenced broadly on Tethyan margins, notably in Italy (Pons and Sirna, 1992; Cestari and Laviano, 2012), Charentes (France; Orbigny, 1822; Bilotte and Philip, 1985; Moreau, 1993; Videt, 2003), Istria (Polšak, 1967; Pleničar et al., 1999; Korbar et al., 2001), Czech Republic (El-Shazly et al., 2011), Jordan (Özer and Ahmad, 2016), Egypt (El-Shazly et al., 2011), Algeria (Chikhi-Aouimeur, 1995, 2003), or Oman (Philip et al., 1995).

The statistical processing of rudist counts as well as the precise description of litho-biofacies allowed us to define stages in the ecological succession of dominant rudist communities, from the settlement of the carbonate platform to its climax. In warm, shallow waters of carbonate platforms, *Ichthyosarcolites* was the first taxon to establish in harsh environments, on unsettled soft substratum. Immediately, the centimetric *Caprotina* settled directly by encrustation on the large of *Ichthyosarcolites* shells, taking advantage of the appearance of a hard substratum to which the larva can attach itself. The sedimentary fabrics of the platform subsequently changed the environmental conditions. The appearance of the 'mud-sticker' *Chondrodonta* and Sauvagesiinae in bouquets or limited biostromes, alongside the recumbent

Ichthyosarcolites, led to the rise of a more stable environment. This diversified community was regularly punctuated by episodes of rapid development of *Caprotina* patches, which covered large amounts of hard substrates in one generation. The stability of the environment eventually led to the strong expansion of *Apricardia*, *Sauvagesia* and *Durania*, which resulted in oligospecific communities. We interpret here the *Apricardia*-Sauvagesiinae community as the climax, as it appears to be the most stable state of the ecological succession. This community is constituted of a continuum between two opposite poles with dominance of either *Apricardia* or Sauvagesiinae. Within this climacic community, *Apricardia* congregations developed in restricted environments, with low sedimentation rate and very shallow water, while Sauvagesiinae congregations has been established through the relative opening and deepening of the environment.

6. Conclusion

The combination of sedimentological and palaeontological analyses of exceptionally rudist-rich limestones within the upper Cenomanian Fontblanche Formation from the South-Provence carbonate platform led to the following main results:

— the overall depositional environment was very shallow (maximum depth of some metres to zero), in the inner peritidal, sheltered and quiet part of the platform;

— the various macrofossil taxa are well preserved so that most of them are regarded as autochthonous or parautochthonous and were living in this same environment;

— the statistical study of the fossil content allowed us to identify four characteristic fossil assemblages (namely the *Chondrodonta* assemblage, the *Apricardia*-Sauvagesiinae assemblage, the *Caprotina* assemblage, and the *Nerinea* assemblage) and to considered them as representative of biotic communities;

— the link between the sedimentary facies and rudist ecotypes put in evidence that biotic parameters played an important role in the succession and behaviour of rudist communities;

— the degree of biocorrosion, seemingly linked to the sedimentation rate, determined the grainy or silty-muddy nature of the substrate (and ruled the apparent species richness);

— the rudist communities that included *Ichthyosarcolites*, which grew preferentially on an unstable silty-muddy substrate, plus *Caprotina* which were encrusting the *Ichthyosarcolites* shells, acted as pioneering on the carbonate platform;

— Sauvagesiinae and *Chondrodonta* developed on the induced stabilised substrate (without disappearance of *Ichthyosarcolites*) and the *Apricardia*-Sauvagesiinae community became dominant, this community representing a potential climax in dynamic equilibrium with the alternant dominance of one or the other taxa;

— the elevators Sauvagesiinae developed preferentially while the sedimentation rate was high, the biocorrosion subsequently weak and the substrate grainy and firm, whereas the clingers *Apricardia* were settled at the best on a silty-muddy substrate resulting from intense biocorrosion during a slowing down sedimentation rate, in the thinnest slice of water, close to emersion.

Our study emphasises the interest in an approach integrating the results of a high-resolution sedimentological analysis as well as a palaeoecological analysis of rudist communities. When reconstructing palaeoenvironments according to their in situ biotic communities, biotic parameters considered from a synecological point of view must be taken into account as well as abiotic parameters. We put in evidence the dynamics of rudist ecosystems by showing faunal successions linked to changes in environmental parameters. Partially controlling the environment, rudists, themselves, were able to set up the conditions for their flourishing development on Cretaceous carbonate platforms.

References

Amico, S., 1978. Recherches sur la Structure du Test des Radiolitidae (Ph.D. thesis). Université de Provence, Marseille, 131pp (in French).

Ayoub-Hannaa, W., Fürsich, F.T., 2011. Functional morphology and taphonomy of Cenomanian (Cretaceous) oysters from the eastern Sinai peninsula, Egypt. Palaeobiodiversity and Palaeoenvironments 91, 197–214.

Bathurst, R.G.C., 1966. Boring algae, micrite envelopes and lithification of molluscan biosparites. Geological Journal 5, 15–32.

Bernier, P., Strasser, A., 1988. Formation de galets noirs et coquilles noircies dans l'actuel (Ile de Noirmoutier, France). Bulletin de la Société Géologique de France 4, 341–347 (in French with English abstract).

Bilotte, M., Philip, J., 1985. Les faunes de rudistes du Crétacé supérieur Charentais du chantier de l'autoroute "l'Aquitaine". Cretaceous Research 6, 79–84 (in French with English abstract).

Brachert, T.C., Dullo, W.C., 2000. Shallow burial diagenesis of skeletal carbonates: selective loss of aragonite shell material (Miocene to recent, Queensland plateau and Queensland

trough, NE Australia). Implications for shallow cool-water carbonates. Sedimentary Geology 136, 169–187.

Carannante, G., Ruberti, D., Simone, L., 1993. Rudists and related sediments in late Cretaceous open shelf settings. A case history from Matese area (central Apennines, Italy). Giornale di Geologia 55, 21–36.

Carannante, G., Graziano, R., Ruberti, D., Simone, L., 1997. Upper Cretaceous temperate-type open shelves from northern (Sardinia) and southern (Apennines-Apulia) Mesozoic Tethyan margins. In: James, N.P., Clarke, J.A.D. (Eds.) Cool-Water Carbonates. SEPM Special publication 56. Society for Sedimentary Geology, Tulsa, pp. 309–325.

Carannante, G., Ruberti, D., Sirna, M., 2000. Upper Cretaceous ramp limestones from the Sorrento peninsula (southern Apennines, Italy): micro-and macrofossil associations and their significance in the depositional sequences. Sedimentary Geology 132, 89–123.

Cestari R., Laviano A., 2012. Rudist facies distribution in the late Cretaceous of Cilento and western Basilicata (southern Italy). Rivista Italiana di Paleontologia e Stratigrafia 118, 277–294.

Chéreau, A., Gruneisen, P., Montenat, C., Soudet, H.J., 1997. A dynamic model of a rudist carbonate platform: the middle Cenomanian of Oléron (France). Bulletin du Centre de Recherches Elf Exploration Production 20, 1–29.

Chikhi-Aouimeur, F., 1995. *Caprinula* aff. *cedrorum* (Blanckenhorn, 1890) from the upper Cenomanian of western Algeria. Revista Mexicana de Ciencias Geológicas 12, 179–184.

Chikhi-Aouimeur, F., 2003. Stratigraphic and geographic distribution of rudists in Algeria: a state of the art. In: Gili, E., El Hédi Negra, M., Skelton, P.W. (Eds.) North African Cretaceous

Carbonate Platform Systems. Kluwer Academic Publishers, Dordrecht, Boston, London, pp. 161–170.

Citton, P., Fabbi, S., Cipriani, A., Jansen, M., Romano, M., 2019. Hybodont dentition from the upper Jurassic of Monte Nerone pelagic carbonate platform (Umbria-Marche Apennine, Italy) and its ecological implications. Geological Journal, 54, 278-290.

Crumière-Airaud, C., 1991. Stratigraphie et Evolutions Sédimentaires des Domaines de Plate-Forme Carbonatée à Rudistes au Cours du Passage Cénomanien-Turonien: Exemples Choisis sur le Domaine Périméditerranéen Actuel (Ph.D. thesis). Université Aix-Marseille I, Marseille, 95pp (in French).

Dalmasso, H., Floquet, M., 2001. Relation accommodation–production carbonatée dans le développement de séquences de dépôt élémentaires de plate-forme carbonatée: la série d'âge Tithonien–Berriasien de basse Provence occidentale. Comptes Rendus de l'Académie des Sciences - Series IIA - Earth and Planetary Science 333, 209–217 (in French with English abstract).

El-Shazly, S., Košťák, M., Kloučková, B., Saber, S.G., Felieh Salama, Y., Mazuch, M., Žák, K., 2011. Carbon and oxygen stable isotopes of selected Cenomanian and Turonian rudists from Egypt and Czech Republic, and a note on changes in rudist diversity. Bulletin of Geosciences 86, 209–226.

Embry, A.F., 2009. Practical Sequence Stratigraphy. Canadian Society of Petroleum Geologists, Calgary, 81pp.

Embry, A.F.I., Klovan, J.E., 1971. A late Devonian reef tract on northeastern Banks Island. Bulletin of Canadian Petroleum Geology 19, 730–781.

Fenerci-Masse, M., Masse, J.P., Pernarcic, E., 2005. Quantitative stratigraphy of rudist limestones and its bearing on spatial organisation of rudist communities: the late Barremian, Urgonian, sequences of Provence (S.E. France). Palaeogeography, Palaeoclimatology, Palaeoecology 215, 265–284.

Floquet, M., 1982. Un modèle de comblement de plate-forme interne carbonatée: Santonien supérieur-Campanien des chaines Ibériques nord. Cretaceous Research 3, 69–81 (in French with English abstract).

Floquet, M., 1990. La Plate-Forme Nord-Castillane au Crétacé Supérieur (Espagne). Arrière-Pays Ibérique de la Marge Passive Basco-Cantabrique. Sédimentation et Vie. Mémoires Géologiques de l'Université de Dijon 14, 925pp (in French).

Floquet, M., 2020. Le Bassin marin sud-Provençal: de son extension à partir du Cénomanien (vers -100 Ma) jusqu'à sa fermeture au Santonien supérieur (vers -84 Ma). In: Bourideys, J. (Ed.), Géologie des Bouches du Rhône. Roches et Paysages Remarquables. BRGM Editions, Orléans, pp. 64–84 (in French).

Floquet, M., Hennuy, J., 2001. Anatomy of a carbonate resedimentation within the latest Turonian–earliest Coniacian south Provençal basin. Géologie Méditerranéenne 28, 67–71.

Floquet, M., Hennuy, J., 2003. Evolutionary gravity flow deposits in the middle Turonian-early Coniacian southern Provence basin (SE France): origins and depositional processes. In: Locat, J., Mienert, J. (Eds.) Submarine Mass Movements and their Consequences, 1st International Symposium. Kluwer Academic Publishers, Dordrecht, Boston, London, pp. 417–424.

Floquet, M., Gari, J., Hennuy, J., Léonide, P., Philip, J., 2005. Sédimentations gravitaires carbonatées et silicoclastiques dans un bassin en transtension, séries d'âge Cénomanien à

Coniacien moyen du bassin sud-Provençal. Publication Association des Sédimentologistes Français 52, 1–80 (in French).

Floquet, M., Philip, J., Léonide, P., Gari, J., 2006. Sédimentation et Géodynamique du Bassin Sud-Provençal au Crétacé Supérieur (Field Trip Guide). Université de Provence / Aix-Marseille I, Marseille, 69pp (in French).

Floquet, M., Léonide, P., Villier, L., Ackouala, A.-P., Blenet, A., 2013. Expressions biosédimentaire, diagénétique, géochimique et tectonique de l'événement anoxique Cénomano-Turonien (OAE 2) par les plateformes carbonatées sud-Provençales. Publication Association des Sédimentologistes Français, 73, 1-145 (in French with English abstract).

Floquet, M., Hennuy, J., Philip, J., 2018. Le Crétacé supérieur. In: Villeneuve, M. (Coord.) Mémoire Explicatif, Carte Géologique de France (1/50 000), Feuille Aubagne-Marseille, 3ème Édition. BRGM Editions, Orléans, pp. 63–81 (in French).

Flügel, 2010. Microfacies of Carbonate Rocks. Analysis, Interpretation and Application. 2nd edition. Springer-Verlag, Berlin, Heidelberg, 984 pp.

Freytet, P., Plaziat, J.C., 1982. Continental carbonate sedimentation and pedogenesis. Late Cretaceous and early Tertiary of southern France. In: Purser, B.H. (Ed.) Contributions to Sedimentology. Schweitzerbartsche Verlagsbuchhandlung, Stuttgart, 213 pp.

Gili, E., Skelton, P.W., 2000. Factors regulating the development of elevator rudist congregations. In: Insalaco, E., Skelton, P.W., Palmer, T. (Eds.) Carbonate Platform Systems: Components and Interactions. Geological Society Special Publications 178. Geological Society, London, pp. 109–116.

Gili, E., Götz, S., 2018. Part N, Volume 1, Chapter 26B: Paleoecology of rudists. Treatise Online 103, 1–29.

Gili, E., Skelton, P. W., Bover-Arnal, T., Salas, R., Obrador, A., Fenerci-Masse, M, 2016. Depositional biofacies model for post-OAE1a Aptian carbonate platforms of the western Maestrat basin (Iberian chain, Spain). Palaeogeography, Palaeoclimatology, Palaeoecology, 453, 101–114.

Gili, E., Masse, J.-P., Skelton, P.W., 1995. Rudists as gregarious sediment-dwellers, not reef-builders, on Cretaceous carbonate platforms. Palaeogeography, Palaeoclimatology, Palaeoecology 118, 245–267.

Goodwin, P.W., Anderson, E.J., 1985. Punctuated aggradational cycles: a general hypothesis of episodic stratigraphic accumulation. The Journal of Geology 93, 513–533.

Guillocheau, F., 1995. Nature, rank and origin of Phanerozoic sedimentary cycles. Comptes Rendus de l'Académie des Sciences de Paris, IIA 320, 1141–1157.

Hammer, Ø., Harper, D.A.T., Ryan, P.D., 2001. PAST: paleontological statistics software package for education and data analysis. Palaeontologia Electronica 4, 1–9.

Hennuy, J., 2003. Sédimentation Carbonatée et Silicoclastique sous Contrôle Tectonique, le Bassin Sud-Provençal et sa Plate-Forme Carbonatée du Turonien Moyen au Coniacien Moyen. Evolutions Séquentielle, Diagénétique, Paleogéographique (Ph.D. thesis). Université de Provence, Marseille, 252 pp (in French).

Janson, X., Lee, K., Zahm, C., Kerans, C, 2015. Ground-penetrating radar imaging of Albian rudist buildups, central Texas. Interpretation 3, 67–81.

Kidwell, S.M., Holland, S.M., 1991. Field description of coarse bioclastic fabrics. Palaios 4, 426–434.

Kidwell, S.M., Holland, S.M., 2002. The quality of the fossil record: implications for evolutionary analyses. Annual Review of Ecology and Systematics 33, 561–588.

Korbar, T., Fucek, L., Husinec, A., Vlahovic, I., Ostric, N., Maticek, D., Jelaska, V., 2001. Cenomanian carbonate facies and rudists along shallow intraplatform basin margin-the island of Cres (Adriatic sea, Croatia). Facies 45, 39–58.

Martill, D. M., Taylor, M. A., Duff, K. L., 1994. The trophic structure of the biota of the Peterborough member, Oxford clay formation (Jurassic), UK. Journal of the Geological Society of London, 151, 173-194.

Martin, R.E., 1999. Taphonomy: a Process Approach. Cambridge University Press, Cambridge, 508pp.

Masse, J.-P., Philip, J., 1976. Paléogéographie et tectonique du Crétacé moyen en Provence: révision du concept d'isthme durancien. Revue de Géographie physique et de Géologie dynamique 18, 49–66 (in French with English abstract).

Masse, J.-P., Philip, J., 1981. Cretaceous coral-rudist buildups of France. In: Toomey, D.F. (Ed.) European Fossil Reef Models. SEPM Special publication 30. Society for Sedimentary Geology, Tulsa, pp. 399–426.

Masse, J.-P., Montaggioni, L., 2001. Growth history of shallow-water carbonates: control of accommodation on ecological and depositional processes. International Journal of Earth Sciences 90, 452–469.

Masse, J.-P., Fenerci, M., Pernarcic, E., 2003. Palaeobathymetric reconstruction of peritidal carbonates. Late Barremian, Urgonian, sequences of Provence (SE France). Palaeogeography, Palaeoclimatology, Palaeoecology 200, 65–81.

Möbius, K.A., 1877. Die Auster und die Austernwirtschaft, Verlag von Wiegandt, Hemple & Parey, Berlin, 126pp (in German).

Moreau, P., 1993. La Transgression Cénomanienne sur la Marge Septentrionale du Bassin de l'Aquitaine (Charentes). Flanc Nord du Synclinal de Saintes et de l'Angoumois. Modalité d'une Invasion Marine (Ph.D. thesis). Université de Poitiers, Poitiers, 1590pp (in French).

Orbigny, A. de, 1822. Notice sur quelques espèces nouvelles de mollusques fossiles, du département de la Charente-Inférieure. Mémoires du Muséum d'Histoire Naturelle 8, 98–110 (in French).

Özer, S., Ahmad, F., 2016. *Caprinula* and *Sauvagesia* rudist faunas (Bivalvia) from the Cenomanian of NW Jordan. Stratigraphy and taxonomy. Cretaceous Research 58, 141–159.

Philip, J., 1967. Les zones de rudistes du Cénomanien Provençal. Bulletin de la Société Géologique de France 7, 497–503 (in French).

Philip, J., 1970. Les Formations Calcaires à Rudistes du Crétacé Supérieur Provençal et Rhodanien. (Thèse d'État). Université de Provence, Marseille, 438 pp (in French).

Philip, J., 1972. Paléoécologie des formations à rudistes du Crétacé supérieur - l'exemple du sud-est de la France. Palaeogeography, Palaeoclimatology, Palaeoecology 12, 205–222 (in French with English abstract).

Philip, J., 1981. Les rudistes du Crétacé moyen de la province Méditerranéenne occidentale. Evolution, paléoécologie, paléobiogéographie. Cretaceous Research 2, 395–403 (in French with English abstract).

Philip, J., 1993. Late Cretaceous carbonate-siliciclastic platforms of Provence, southeastern France. In: Simo, J.A.T., Scott, R.W., Masse, J.-P. (Eds.) Cretaceous Carbonate Platforms, Memoirs of the American Association of Petroleum Geologists 56, Tulsa, pp. 375–385.

Philip, J., 1998. Sequences and systems tracts of mixed carbonate-siliciclastic platform-basin settings: the Cenomanian-Turonian stages of Provence (southeastern France). In: Graciansky,

P.C. de, Hardenbol, J., Jacquin, T., Vail, P.R. (Eds.) Mesozoic and Cenozoic Sequence Stratigraphy of European Basins. SEPM Special publication 60. Society for Sedimentary Geology, Tulsa, pp. 387–395.

Philip, J., Airaud, C., Tronchetti, G., 1989. Événements paléogéographiques en Provence (SE France) au passage Cénomanien-Turonien. Modifications biosédimentaires - causes géodynamiques. Geobios 22, 107–117 (in French with English abstract).

Philip, J., Airaud-Crumière, C., 1991. The demise of the rudist-bearing carbonate platforms at the Cenomanian/Turonian boundary: a global control. Coral Reefs 10, 115–125.

Philip, J., Borgomano, J., Al-Maskiry, S., 1995. Cenomanian-early Turonian carbonate platform of northern Oman: stratigraphy and palaeo-environments. Palaeogeography, Palaeoclimatology, Palaeoecology 119, 77–92.

Pleničar, M., Jurkovšek, B., Kolar-Jurkovšek, T., 1999. Stop 1: Cenomanian-Turonian bioherm on Hrušica. In: Höfling, R., Steuber, T. (Eds.) Fifth International Congress on Rudists: Ab-stracts and Field Trip Guides. Erlanger geologische Abhandlungen, Sonderband, pp. 118-121.

Polšak, A., 1967. Kredna makrofaun a južne Istre - Macrofaune Crétacée de l'Istrie méridionale (Yougoslavie). Jugloslavenska Akademija Znanosti I Umjetnosti 8, 147-187 (In Croatian with French translation).

Pons, J.M., Sirna, G., 1992. Upper Cretaceous rudists distribution in the mediterranean Tethys: comparison between platforms from Spain and south-central Italy. Geologica Romana 28, 341–350.

Posenato, R., Frijia, G., Morsilli, M., Moro, A., Del Viscio, G., Mezga, A., 2020. Paleoecology and proliferation of the bivalve *Chondrodonta joannae* (Choffat) in the upper

Cenomanian (upper Cretaceous) Adriatic carbonate platform of Istria (Croatia). Palaeogeography, Palaeoclimatology, Palaeoecology 548, 2–15.

R Core Team, 2020. R: a language and environment for statistical computing. R Foundation for Statistical Computing, Vienna. https://www.R-project.org (2021).

Rameil, N., Immenhauser, A., Warrlich, G., Hillgärtner, H., Droste, H.J., 2010. Morphological patterns of Aptian *Lithocodium-Bacinella* geobodies: relation to environment and scale. Sedimentology 57, 883–911.

Redondo, C., 1986. Étude des Sédiments Détritiques du Crétacé Supérieur Marin de la Provence Occidentale et Recherche des Zones d'Apport. Sédimentologie ; Pétrographie ; Minéralogie (Ph.D. thesis). Université de Provence, Marseille, 474pp (in French).

Rineau, V., 2017. Un Nouveau Regard Cladistique sur l'Anatomie Comparée, la Phylogénie, la Systématique et la Paléoécologie des Rudistes (Bivalvia, Hippuritida) (Ph.D. thesis). Université Pierre et Marie Curie, Paris, 624pp (in French with English abstract).

Rineau, V., Masse, J.-P., Villier, L., 2020. A new cladistic insight on comparative anatomy and phylogeny of rudists (Bivalvia, Hippuritida). Journal of Systematic Palaeontology 18, 1243–1297.

Roduit, N., 2008. JMicroVision version 1.2.7: Image analysis toolbox for measuring and quantifying components of high-definition images. https://jmicrovision.github.io (2021).

Ross, D., Skelton, P., 1993. Rudist formations of the Cretaceous: a palaeoecological, sedimentological and stratigraphical review. In: Wright, P. (Ed.) Sedimentology Review. Blackwell Scientific Publications, Oxford, pp. 73–91.

Ruberti, D., 1997. Facies analysis of an upper Cretaceous high-energy rudist-dominated carbonate ramp (Matese mountains, central-southern Italy): subtidal and peritidal cycles. Sedimentary Geology 113, 81–110.

Sanders, D., 1999. Shell disintegration and taphonomic loss in rudist biostromes. Lethaia 32, 101–112.

Sanders, D., 2001. Burrow-mediated carbonate dissolution in rudist biostromes (Aurisina, Italy): implications for taphonomy in tropical, shallow subtidal carbonate environments. Palaeogeography, Palaeoclimatology, Palaeoecology 168, 39–74.

Scott, R.W., 1995. Cretaceous rudists of Guatemala. Revista Mexicana de Ciencias Geológicas 12, 294–306.

Seilacher, A., 1984. Constructional morphology of bivalves: evolutionary pathways in primary versus secondary soft-bottom dwellers. Palaeontology 27, 207–237.

Skelton, P.W., 1978. The evolution of functional design in rudists (Hippuritacea) and its taxonomic implications. Philosophical Transactions of the Royal Society B: Biological Sciences 284, 305–318.

Skelton, P.W., 1991. Morphogenetic versus environmental cues for adaptive radiations. In: Schmidt-Kittler, N., Vogel, K. (Eds.) Constructional Morphology and Evolution. Springer-Verlag, Berlin, Heidelberg, pp. 375–388.

Skelton, P. W., 2003. Rudist evolution and extinction - a north African perspective. In: Gili, E., El Hédi Negra, M., Skelton, P.W. (Eds.) North African Cretaceous Carbonate Platform Systems. Kluwer Academic Publishers, Dordrecht, Boston, London, pp. 215–227.

Skelton, P.W., Masse, J.-P., Alsharhan, A.S., Scott, R.W., 2000. Synoptic guide to lower Cretaceous rudist bivalves of Arabia. In: Alsharhan, A.S., Scott, R.W. (Eds.) Middle East

Models of Jurassic/Cretaceous Carbonate Systems. SEPM Special publication 69. Society for Sedimentary Geology, Tulsa, pp. 89–99.

Smith, A.M., Nelson, C.S., 2003. Effects of early sea-floor processes on the taphonomy of temperate shelf skeletal carbonate deposits. Earth-Science Reviews 63, 1–31.

Stampfli, M., 1993. Le Briançonnais, terrain exotique dans les Alpes? Eclogae Geologicae Helvetiae 86, 1–45 (in French).

Steuber, T., Löser, H., 2000. Species richness and abundance patterns of Tethyan Cretaceous rudist bivalves (Mollusca: Hippuritacea) in the central-eastern Mediterranean and Middle East, analysed from a palaeontological database. Palaeogeography, Palaeoclimatology, Palaeoecology 162, 75–104.

Steuber, T., Scott, R.W., Mitchell, S.F., Skelton, P.W., 2016. Part N, revised, volume 1, chapter 26C: stratigraphy and diversity dynamics of Jurassic-Cretaceous Hippuritida (rudist bivalves). Treatise Online 81, 1–17.

Strasser, A., Davaud, E., 1983. Black pebbles of the Purbeckian (Swiss and French Jura): lithology, geochemistry and origin. Eclogae Geologicae Helvetiae 76, 551–580.

Tomasovych, A., Schlogl, J., 2008. Analyzing variations in cephalopod abundances in shell concentrations: the combined effects of production and density-dependent cementation rates. Palaios 23, 648–666.

Videt, B., 2003. Dynamique des Paléoenvironnements à Huîtres du Crétacé Supérieur Nord-Aquitain (SO France) et du Mio-Pliocène Andalou (SE Espagne): Biodiversité, Analyse Séquentielle, Biogéochimie (Ph.D. thesis). Université Rennes 1, Rennes, 264pp (in French).

Villier, L., 2009. Linking evolution of fossil communities with evolution of carbonate sedimentary systems. Palaios 24, 551–552.

Wright, V.P., 1994. Paleosols in shallow marine carbonate sequences. Earth-Science Reviews 35, 367–395.

Wright, V.P., Tucker, M.E., 1991. Calcretes: an introduction. International Association of Sedimentologists, Reprint Series 2, 1–22.

Figures captions

Figure 1. Geographical and geological setting. A: Location of the study area in southeastern France, between the cities of Marseille (M) and Toulon (T). B: Palaeogeographical sketch of western Europe during the late Cenomanian to Coniacian and place of the South-Provence Basin (SPB) to the northeastern rim of the Pyreneo-Provencal Rift. C: Detail of the South-Provence Basin during the late Cenomanian; location of the Bastide d'Orves (BO), Barre des Aiguilles (BA) and Fontblanche (FB) sections (black stars) and of the cities of Marseille (M) and Toulon (T) (black dots). White: emerged land; yellow: coastal environment; light blue: carbonate platform; green: outer shelf; dark blue: deep sea. B and C modified from Floquet and Philip (2018), after Stampfli (1993), Floquet and Hennuy (2001), Hennuy (2003), Floquet et al. (2005, 2006).

Figure 2 - Bastide d'Orves (BO) section. Upper part of Fontblanche 1 Unit (upper Cenomanian), Fontblanche 2 Unit (U.m.C. = uppermost Cenomanian to L.m.T. = lowermost Turonian) and Nodosoides Bearing Nodular Limestones (NBNL) Formation (L.T. = Lower Turonian). Lithology, depositional sequences, biotic assemblages, textures, species richness, percentage of bioclasts, dominance. $S_{BO}1$ to $S_{BO}6$: elementary depositional sequences. $D_{BO}1$ to $D_{BO}6$ plus D_{BO}: sedimentary unconformities. A, B, C, D: biotic assemblages (BA) (A: *Nerinea* BA, B: *Apricardia*-Sauvagesiinae BA, C: *Caprotina* BA; D: *Chondrodonta* BA).

Figure 3 - Barre des Aiguilles (BA) section. Fontblanche 1 Unit (upper Cenomanian) and Fontblanche 2 Unit (U.m.C. = uppermost Cenomanian to L.m.T. = lowermost Turonian). Lithology, depositional sequences, biotic assemblages, textures, species richness, percentage of bioclasts, dominance. $S_{BA}1$ to $S_{BA}5$: elementary depositional sequences. $D_{BA}1$ to $D_{BA}5$ plus D_{BA}: sedimentary unconformities. S.S.F.: Strike Slip Fault. A, B, C, D: biotic assemblages

(BA) (A: *Nerinea* BA, B: *Apricardia*-Sauvagesiinae BA, C: *Caprotina* BA; D: *Chondrodonta* BA). Symbols as in Fig. 2.

Figure 4 - Textures and bioclasts from the Bastide d'Orves section limestones (position of the samples in Fig. 2). A-Sample a2: floatstone with fragmented, bioeroded (macro- and microborings) and recrystallised heterometric bioclasts in a microbioclastic and micritic matrix, G = gastropod shell recrystallised in sparite, S = cellular test of Radiolitidae (probable Sauvagesiinae), Chae = Chaetetidae. B-Sample a4: floatstone with fragmented heterometric bioclasts in a microbioclastic matrix, S = cellular test of Sauvagesiinae. C-Sample a15: packstone-floatstone with fragmented (unrounded) heterometric bioclasts in a microbioclastic and micritic matrix. D-Sample a19: packstone-floatstone with coarse bioeroded bioclasts (borings C) within a dominant microbioclastic matrix. E-Sample a23: packstone with biocorroded and micritised heterometric bioclasts including benthonic foraminifera (Pl = *Planispira* sp., Qu = *Quinqueloculina* sp., Pe = peloid from micritisation of foraminifera). F-Sample a27: packstone (to wackestone) with heterometric broken (unrounded) and biocorroded bioclasts (microborings) in a micritic matrix including microbioclasts (G = gastropod remain recrystallised in sparite). G-Sample a32 (Fontblanche 2 Unit): fine bioclastic packstone recrystallised in biomicrosparite, including fine debris of echinoderms (crinoids), bryozoans, bivalves, *Pithonella, Heterohelix*… plus grains of glauconite (G) and quartz. Scales: 1 mm.

Figure 5 - Textures and bioclasts from the Barre des Aiguilles section limestones (position of the samples in Fig. 3). A-Sample b14: packstone-floatstone with bioeroded heterometric bioclasts (sponge borings Bp and microborings) within a microbioclastic and micritic matrix rich in benthonic foraminifera (P = remains of *Praealveolina* gr. *cretacea*). B-Samples b24: peloidal packstone-floatstone with biocorroded (micrite envelope C) bioclasts recrystallised in sparite plus numerous and partly micritised benthonic foraminifera (Ps = *Pseudolituonella* sp.,

D = *Dicyclina* sp., Nz = *Nezzazatinella* cf. *picardi*, Qu = *Quinqueloculina* sp.). C-Sample b27: packstone-floatstone with coarse bioeroded debris of Radiolitidae (C showing borings and microborings) within a finely microbioclastic and micritic matrix. D-Sample b28: microbioclastic packstone to wackestone with benthonic foraminifera (Qu = *Quinqueloculina* sp., T = *Textularia* sp., Cu = *Cuneolina pavonia*), Styl = styloliths). E-Sample b35 (from Fontblanche 2 Unit): floatstone with coarse debris of Sauvagesiinae (S). G-*Durania* within a bioclastic matrix essentially made of heterometric and fragmented remains of rudists (probably the same Sauvagesiinae), plus peloïds (Pf). F-Sample b40 (from "A4 Unit" *sensu* Hennuy, 2003 or "Dent de Chat Quartzose Calcarenite Formation" *sensu* Floquet et al., 2018, of early Coniacian): quartzose packstone with micritised bioclasts and 30 to 40 % of quartz (Q, from 300 μm up to 1 mm in size). This formation unconformably overlies the upper Cenomanian-lowermost Turonian Fontblanche 2 Unit, with a cartographic discordance. Scale: 1 mm.

Figure 6 - Taxa encountered in Fontblanche 1 microfacies from the Bastide d'Orves and Barre des Aiguilles sections (position of the samples in Figs. 2 and 3). A-Sample a4: Sauvagesiinae, B-Sample a11: *Ichthyosarcolites* sp., C-Sample b19: *Apricardia* sp., D-Sample b19: *Chondrodonta* sp., E-Sample a2: Gastropoda and Radiolitidae, F-Sample a11: *Polystrata alba* (Rhodophyta), G-Sample a8: *Bacinella*, H-Sample b23: Bryozoa, I-Sample b19: Chaetetidae (Porifera), J-Sample a9: *Lithocodium aggregatum* (synonym of *Bacinella irregularis*), K-Sample a9: *Acicularia* sp. (Dasycladaceae), L-Sample b28: *Solenomeris* sp.? (benthonic foraminifera Acervulinidae). Scale: 500 μm.

Figure 7 - Foraminifera (A to S) and dinoflagellate cyst (T) found in Fontblanche 1 microfacies from the Bastide d'Orves and Barre des Aiguilles sections. A-Sample a2: *Triloculina* sp., B-Sample a10: *Quinqueloculina* sp., C-Sample a10: *Pseudolituonella* sp., D-Sample b30: *Spirocyclina* sp., E-Sample a9: *Textularia* sp., F-Sample b30: *Nezzazatinella*

picardi, G-Sample b28: *Cuneolina pavonia*, H-Sample a9: *Charentia* sp., I-Sample b30: *Chrysalidina gradata*, J-Sample b14: *Praealveolina* gr. *cretacea*, K-Sample b19: *Dictyopsella* sp, L-Sample a19: *Planispira* sp., M-Sample b32: *Rotalia mesogeensis*, N-Sample b3: *Tritaxia pyramidata*, O-Sample b20: *Frondicularia* sp., P-Sample a2: *Heterohelix globulosa*, Q-R-Samples b29, b14: *Muricohedbergella* sp., S-Sample b27: ?*Whiteinella* sp., T-Sample b32: *Pithonella sphaerica*. Scale: 100 μm.

Figure 8 - Macrofossils of Fontblanche 1 Unit from the Bastide d'Orves and Barre des Aiguilles sections. A-*Sauvagesia sharpei* (F/ Radiolitidae, sF/ Sauvagesiinae; Bastide d'Orves section); B-*Apricardia* sp. (F/ Requienidae; Bastide d'Orves section), C-*Caprotina* sp. (F/ Caprotinidae; Barre des Aiguilles section); D-*Ichthyosarcolites bicarinatus* (F/ Ichthyosarcolitidae; Barre des Aiguilles section); E-*Chondrodonta joannae* (F/ Chondrodontidae; Barre des Aiguilles section); F-*Nerinea* sp. (F /Nerineidae; Bastide d'Orves section). Scale: 1 cm.

Figure 9 - Macrofossils of Fontblanche 1 Unit from the Bastide d'Orves and Barre des Aiguilles sections. A-*Caprinula boissyi* (F/ Caprinulidae) (the shell, mainly aragonitic, was early dissolved and the resulting void filled with bioclastic and glauconitic dark packstone; Bastide d'Orves section); B-Chaetetidae (Ph/ Porifera; Barre des Aiguilles section), C-Cyclostomata (Ph/ Bryozoa; Barre des Aiguilles section), D-Cidaroida (Ph/ Echinoidea; Barre des Aiguilles section). Scale: 1 cm.

Figure 10 - Taxa frequencies from counting in Fontblanche 1 Unit from the Bastide d'Orves section (BO; macrosamples A1-20). The Sauvagesiinae are mainly represented by the genus *Sauvagesia*.

Figure 11 - Taxa frequencies from counting in Fontblanche 1 Unit from the Barre des Aiguilles section (BA; macrosamples B1-20). Significance of the colours is given by the

coloured boxes of Fig. 10. The Sauvagesiinae are mainly represented by the genus *Sauvagesia*.

Figure 12 - Hierarchical Ascending Classification on taxa frequencies in Fontblanche 1 Unit from the Bastide d'Orves and Barre des Aiguilles sections. Four assemblages are discriminated: A-assemblage with dominant *Chondrodonta* accompanied by *Ichthyosarcolites*, *Caprotina* and Sauvagesiinae; B-assemblage with dominant *Apricardia* and/or Sauvagesiinae; C-assemblage with dominant *Caprotina*; D-assemblage with dominant *Nerinea*. Significances of the colours is given by the coloured boxes of Fig. 10.

Figure 13 - Above: The four biotic assemblages as evidenced by Non-Metric Multidimensional Scaling and illustrating similarities between the counting points of the assemblages in a two-dimensional space (stress: 0.129). Below: illustrations of the four biotic assemblages. A-*Chondrodonta* (Ch) assemblage (Barre des Aiguilles section); B-*Apricardia*-Sauvagesiinae assemblage (A: *Apricardia*; S: Sauvagesiinae, mainly G/ *Sauvagesia*; Bastide d'Orves section); C-*Caprotina* (Cap) assemblage including *Ichthyosarcolites* (Ich) (Barre des Aiguilles section); D-*Nerinea* (N) assemblage (Barre des Aiguilles section). Scale: 5 cm.

Supplementary material

SM 1 - Distribution of various taxa recognised in microfacies from the Bastide d'Orves section (BO).

SM 2 - Distribution of various taxa recognised in microfacies from the Barre des Aiguilles section (BA).

SM 3 - Table of counting frequencies using quadrats from the Bastide d'Orves (macrosamples A1 to A20) and the Barre des Aiguilles (macrosamples B1 to B20).

SM 4 - Unconformities bounding the Fontblanche 1 elementary depositional sequences in the Bastide d'Orves section. A-Unconformity $D_{BO}1$ between $S_{BO}1$ and $S_{BO}2$ (black arrows): reworking of the top of $S_{BO}1$ and overlying rudstone with numerous blackened shells that infiltrate down inside $S_{BO}1$ (at the base of $S_{BO}2$, ghost of *Caprinula* C after shell dissolution). B, C and D-Unconformity $D_{BO}3$ between $S_{BO}3$ and $S_{BO}4$: B-top of $S_{BO}3$ showing a network of dissolution voids (from open factures, aragonitic layer of rudist shells) infilled with a dark green (brown after oxidation) glauconitic, lithoclastic and bioclastic sediment (plus infilling in the internal cavity of rudist shells); C-detail of B exhibiting dissolution of the wall of an open fracture and the filling of the solution cavity with the down-infiltrated dark lithoclastic sediment; D-detail of voids from dissolution of the aragonitic inner layer of *Caprinula* shells and from fractures and of their subsequent infillings.

SM 5 - Unconformities bounding the Fontblanche 1 elementary depositional in the Bastide d'Orves section. A-Unconformity $D_{BO}2$ between $S_{BO}2$ and $S_{BO}3$ (black arrows): wackestone with thin root traces, open burrows, borings and reworking at the top of $S_{BO}2$, and overlying rudist rich floatstone constituting the base of $S_{BO}3$. B-Unconformity $D_{BO}4$ between $S_{BO}4$ and $S_{BO}5$ (black arrows): dissolution of $S_{BO}4$ rudist shells, erosion-truncation of the hardened (bored) top of $S_{BO}4$, reworking of the $S_{BO}4$ rudists within the base of $S_{BO}5$, infiltration of $S_{BO}5$ basal facies down within $S_{BO}4$. C-Unconformity $D_{Bo}6$ between $S_{Bo}6$ at the top of Fontblanche 1 and Fontblanche 2, which resulted from severe erosion-truncation of the Fontblanche 1 rudist bearing limestones and which is highlighted by the drastic faciologic change (Fontblanche 2 bioturbated and nodular fine packstone above) so that $D_{Bo}6$ is regarded as a major sequence boundary.

SM 6 - Unconformities bounding the Fontblanche 1 elementary depositional sequences. A-Detail, on a polished slab, of the $D_{BO}6$ unconformity which separates Fontblanche 1 and Fontblanche 2 in the Bastide d'Orves section: hardground characterised by borings (bo.), iron

oxide crust, oyster encrustation; dissolution (di.) of rudist shells below $D_{BO}6$ except the calcitic outer layer of *Sauvagesia* shells (S.); infilled fine glauconitic packstone of the Fontblanche 2 (in.) down within dissolution voids. B-Unconformity $D_{BA}1$ between $S_{BA}1$ and $S_{BA}2$ in the Barre des Aiguilles section: erosion and reworking underlined by an irregular breccia comprising black and beige pebbles within a matrix including carbonate glaebules and quartz which infiltrate down. C-Unconformity $D_{BA}5$, between $S_{BA}5$ at the top of Fontblanche 1 and Fontblanche 2, in the Barre des Aiguilles section: erosion-truncation at the top of $S_{BA}5$ (black arrow), dense network of dissolution cavities of shells of rudists (*Sauvagesia* S.; see detail in the inset) and of gastropods Nerineidae (N.), and from burrows and fractures; infilling of the cavities with a sediment including quartz and amber-colored fine vegetal remains.

Declaration of interests

☒ The authors declare that they have no known competing financial interests or personal

relationships that could have appeared to influence the work reported in this paper.

☐The authors declare the following financial interests/personal relationships which may be
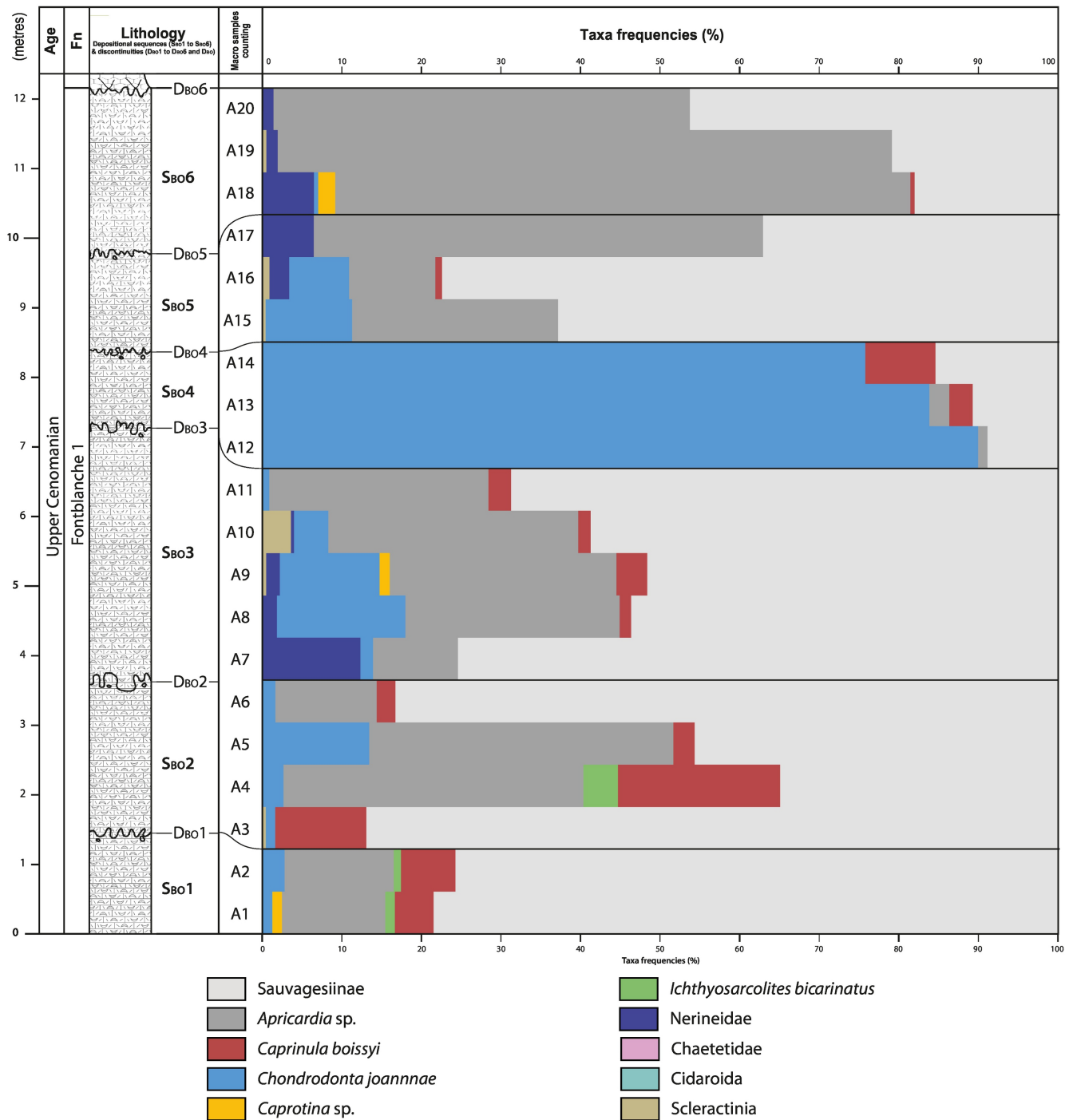considered as potential competing interests:
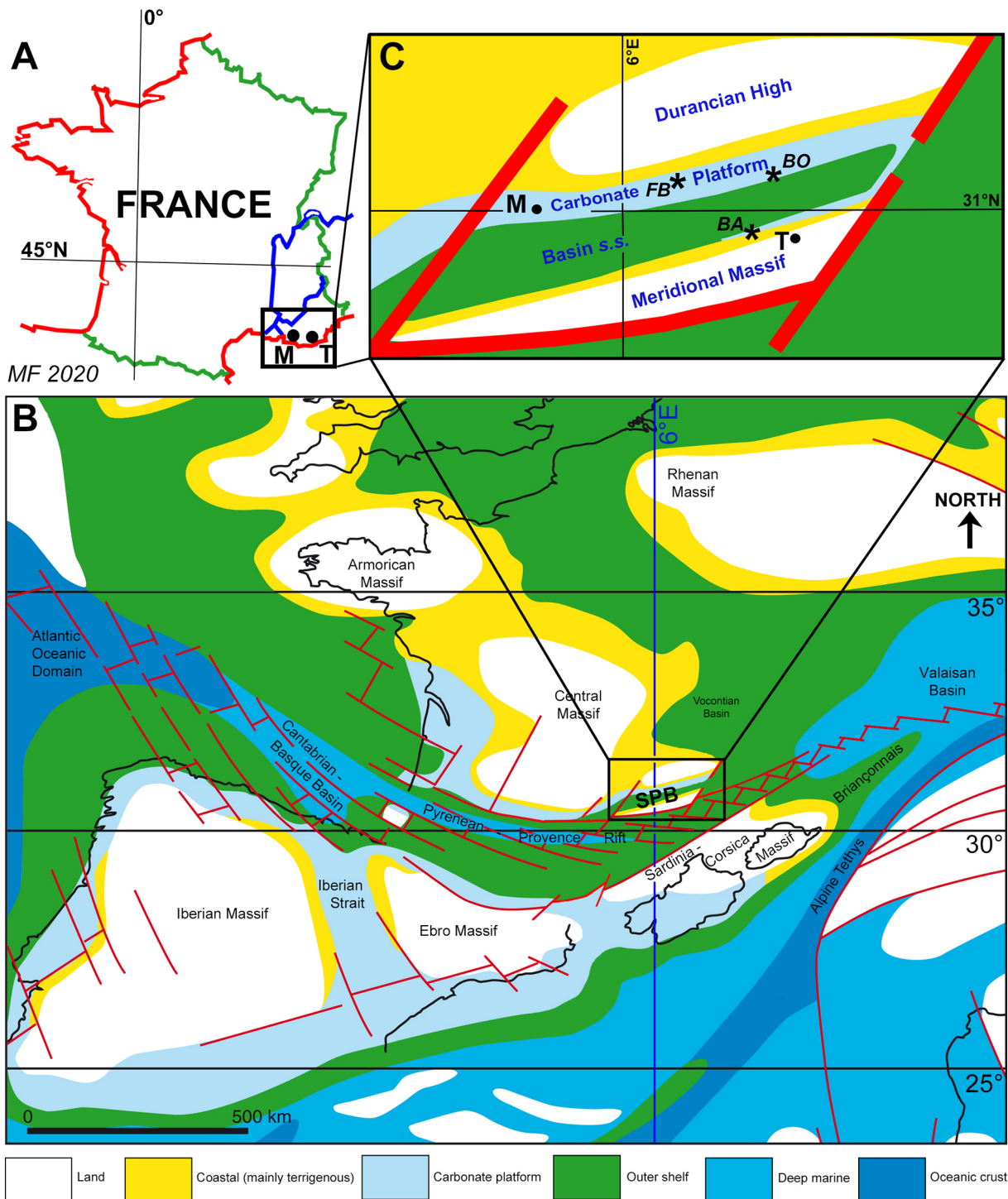
Figure 1
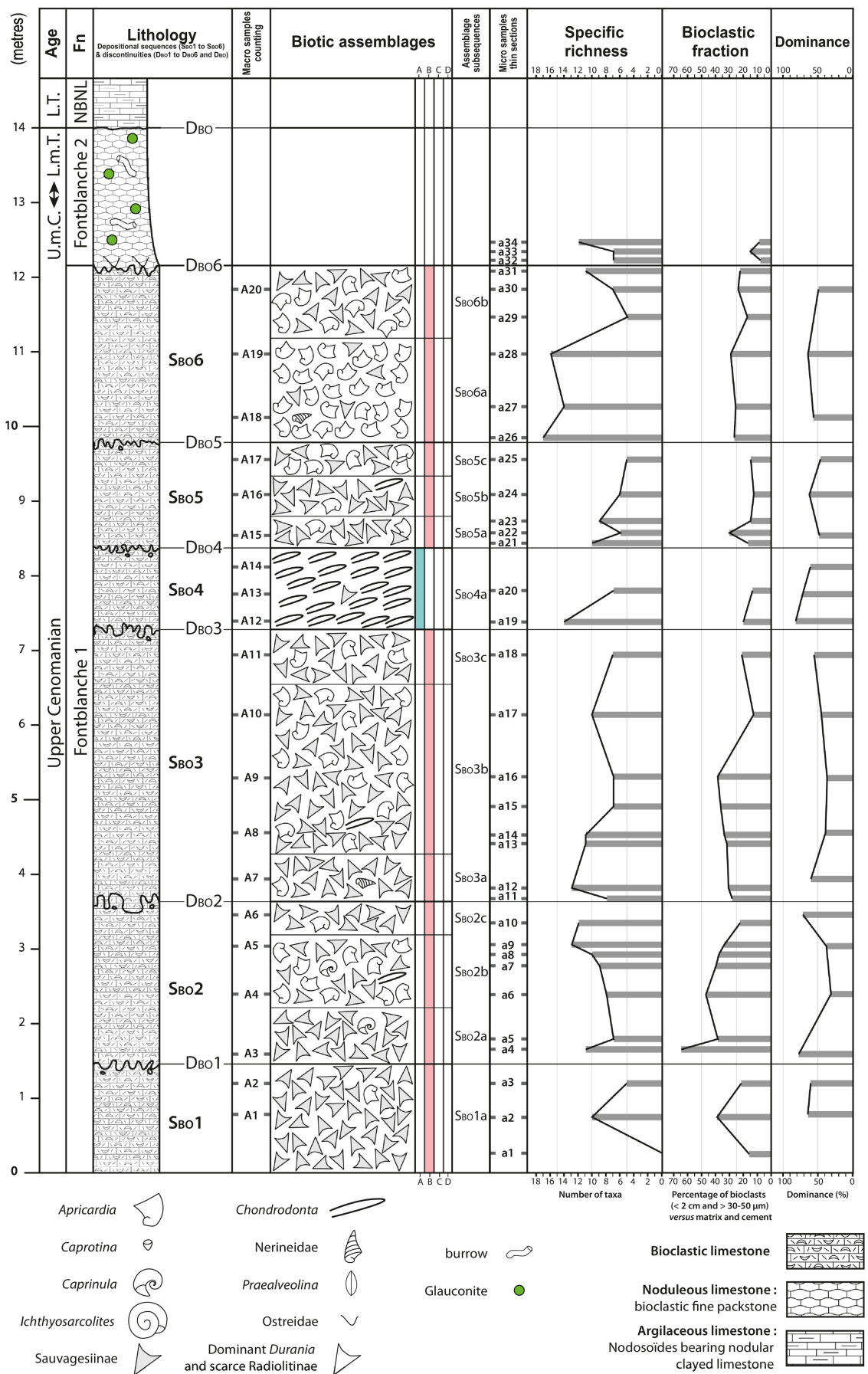
Figure 2
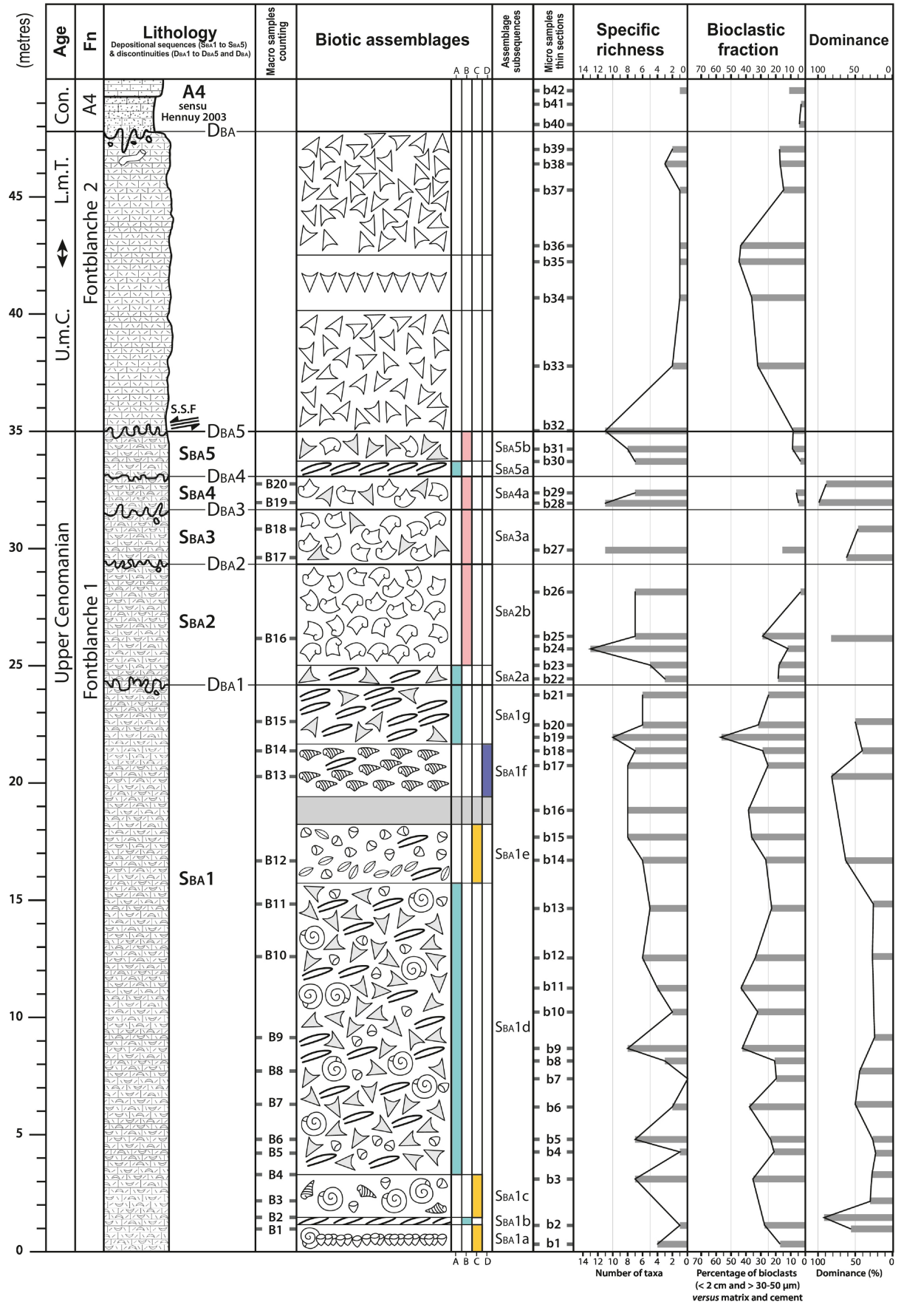
Figure 3
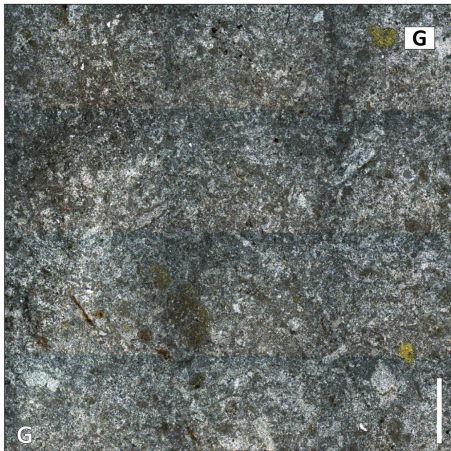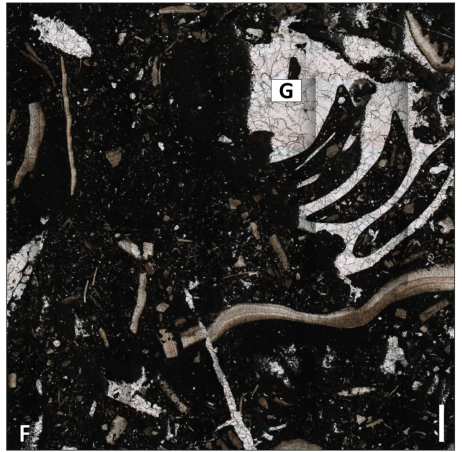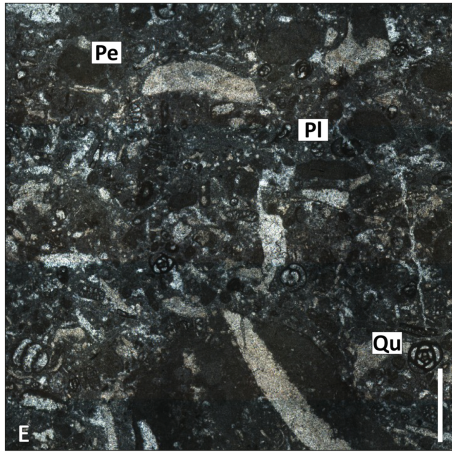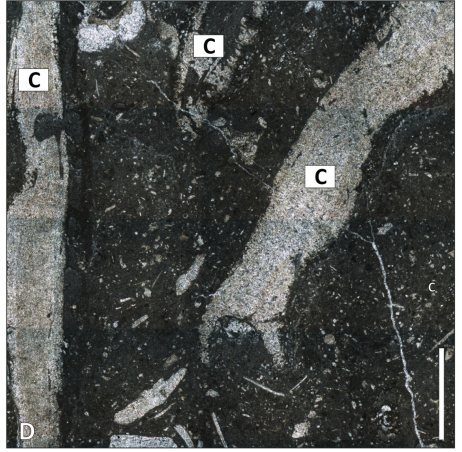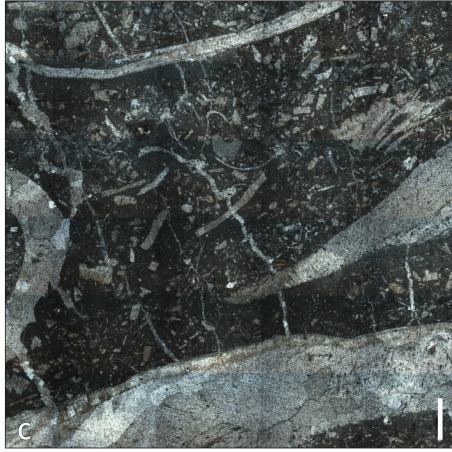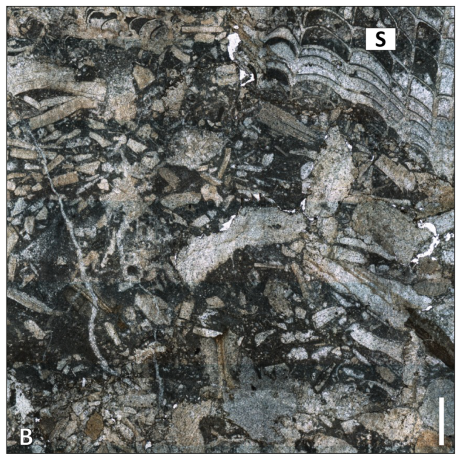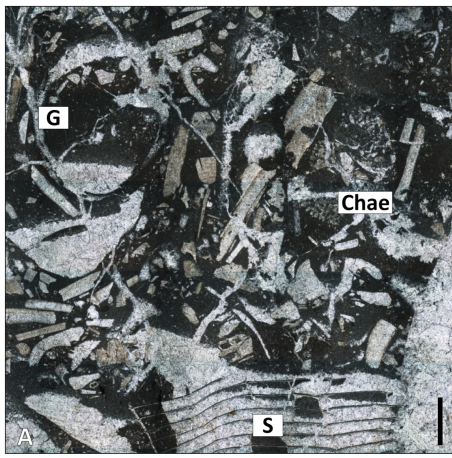
Figure 4
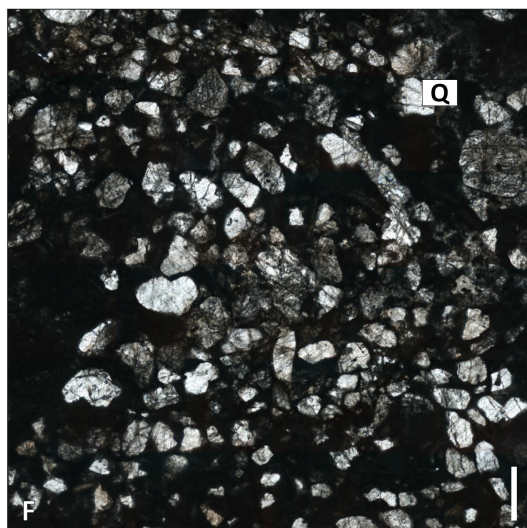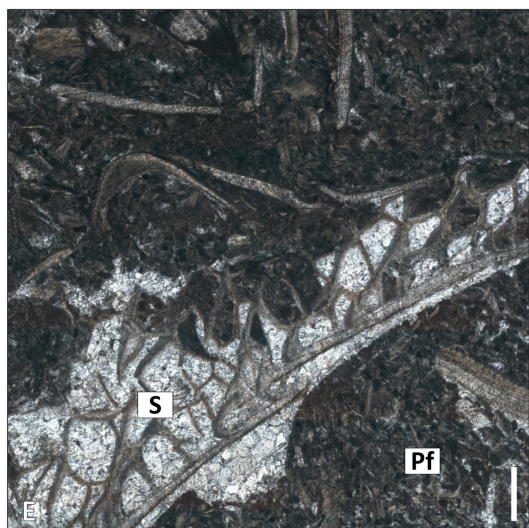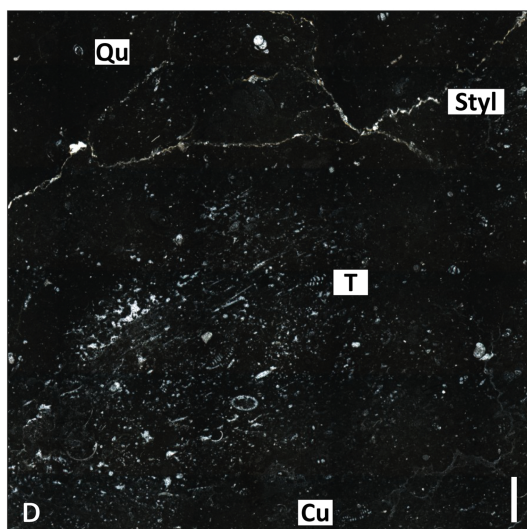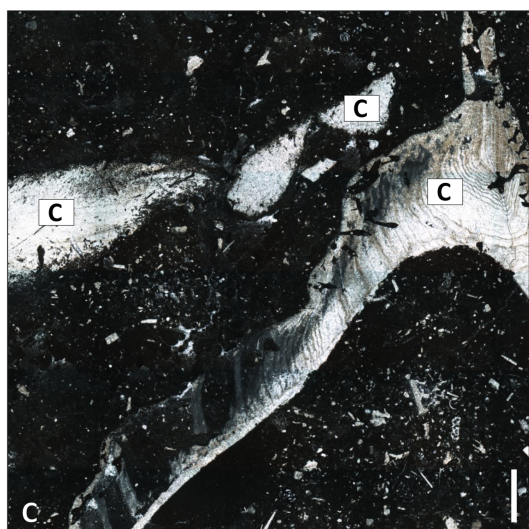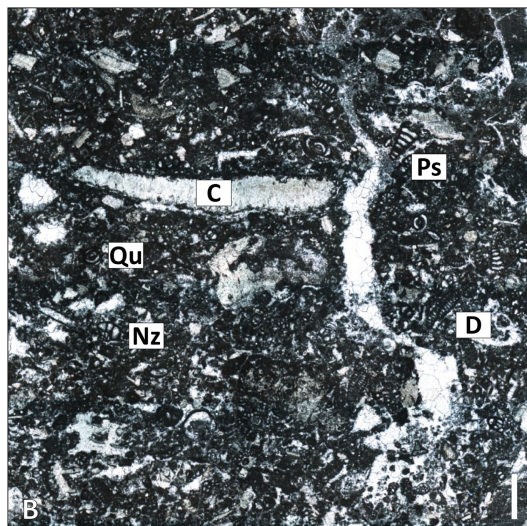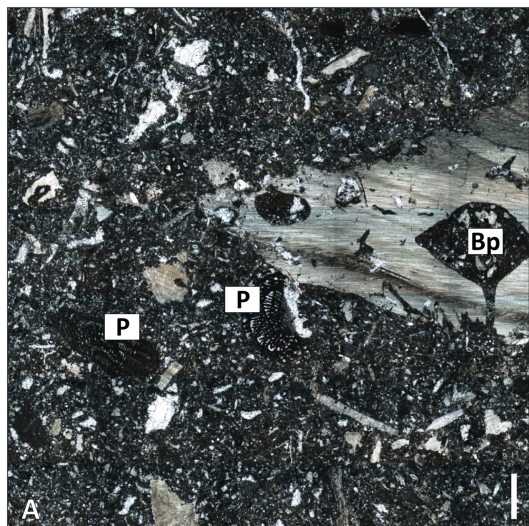
Figure 5
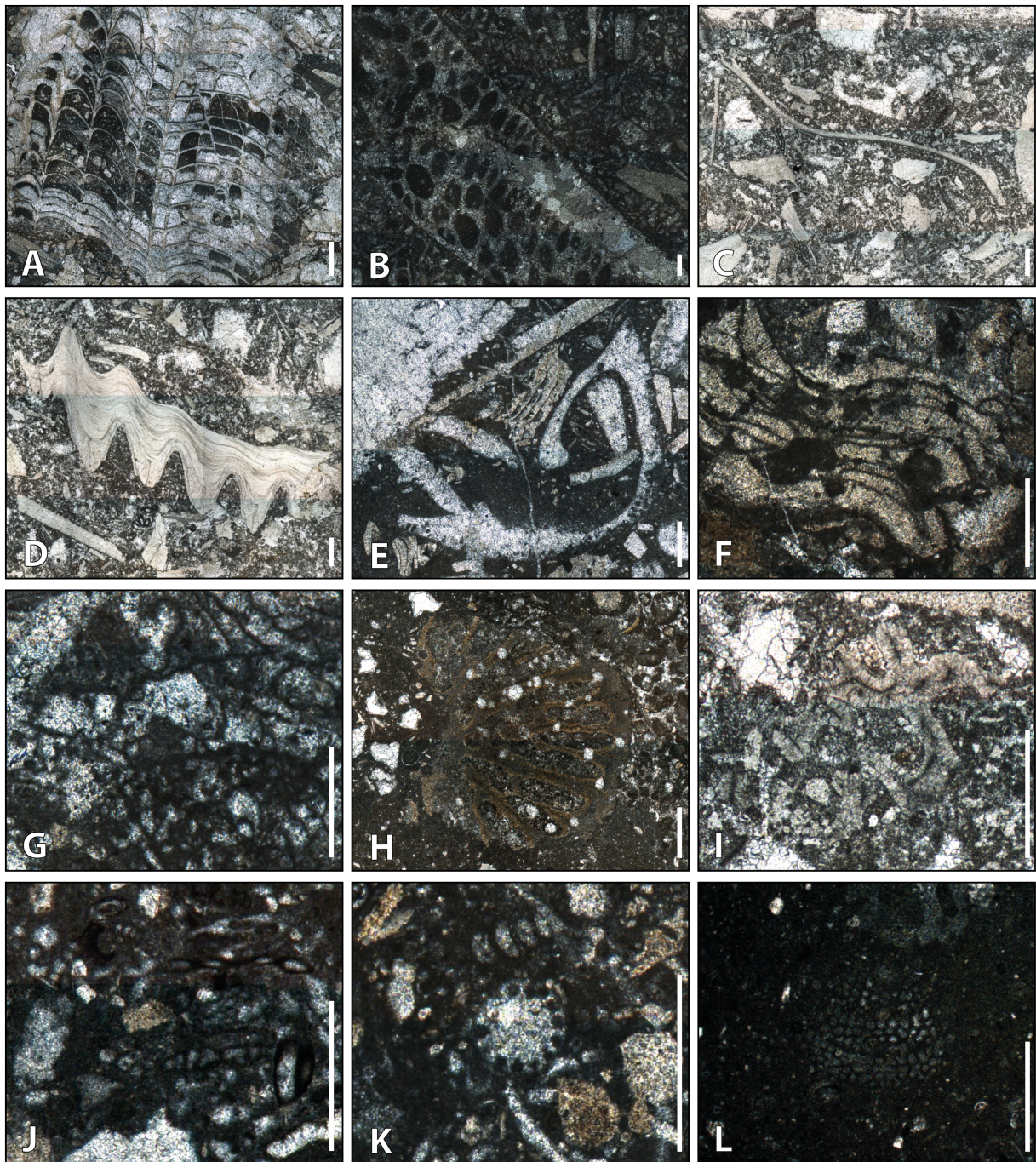
Figure 6
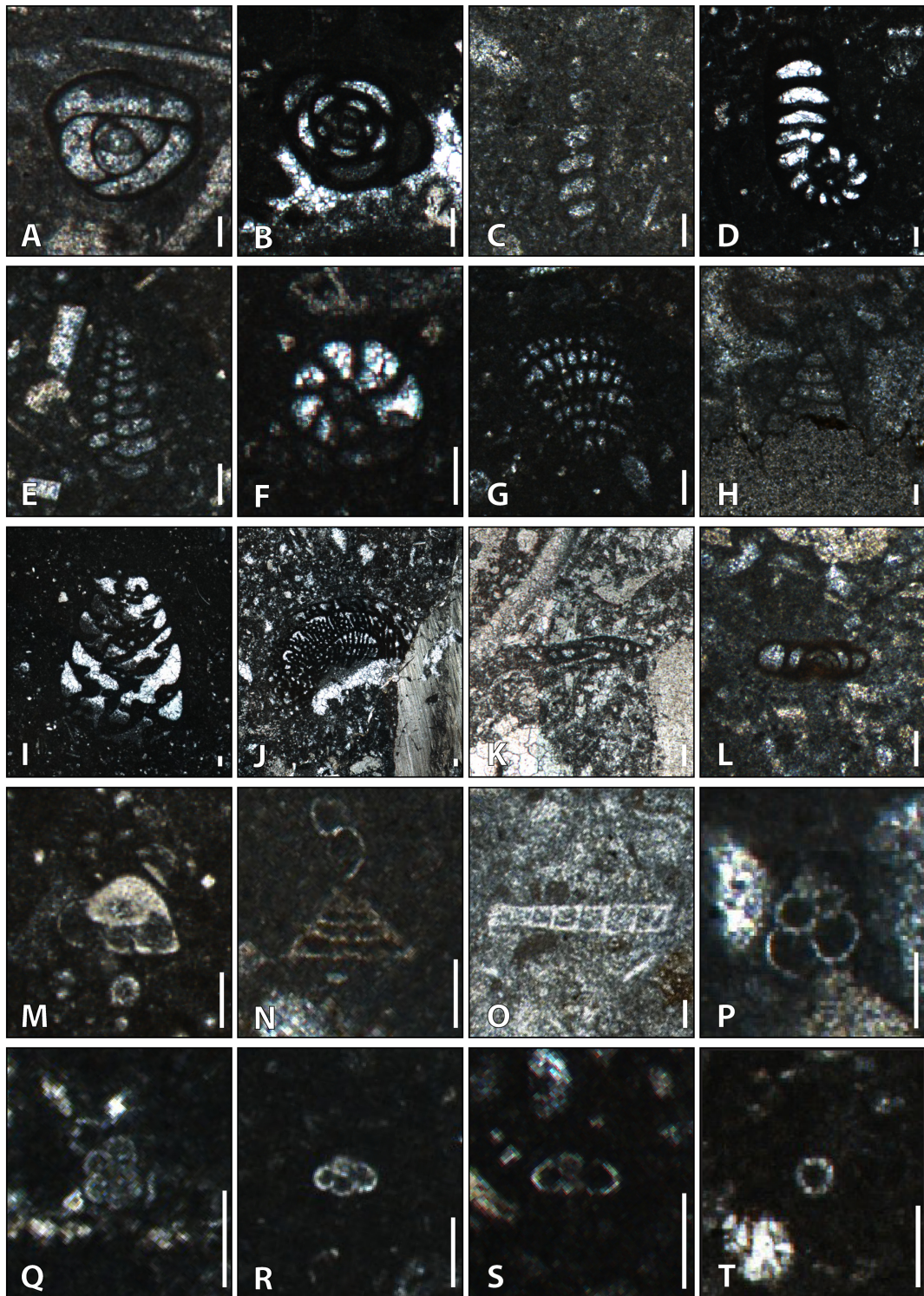
Figure 7
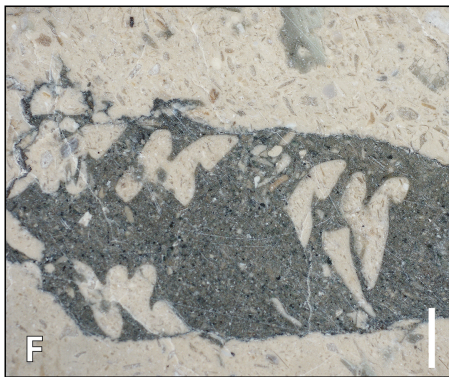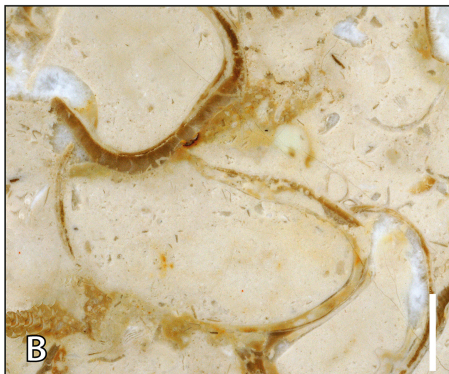
Figure 8
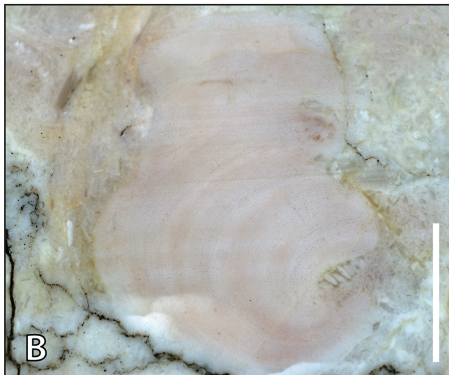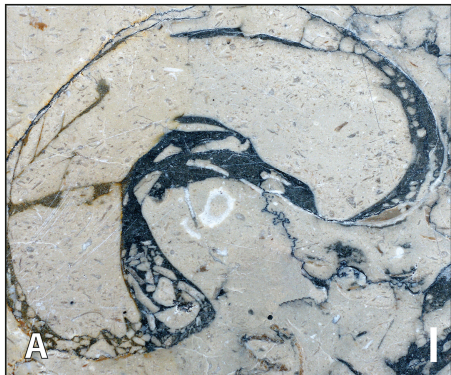
Figure 9

Figure 10
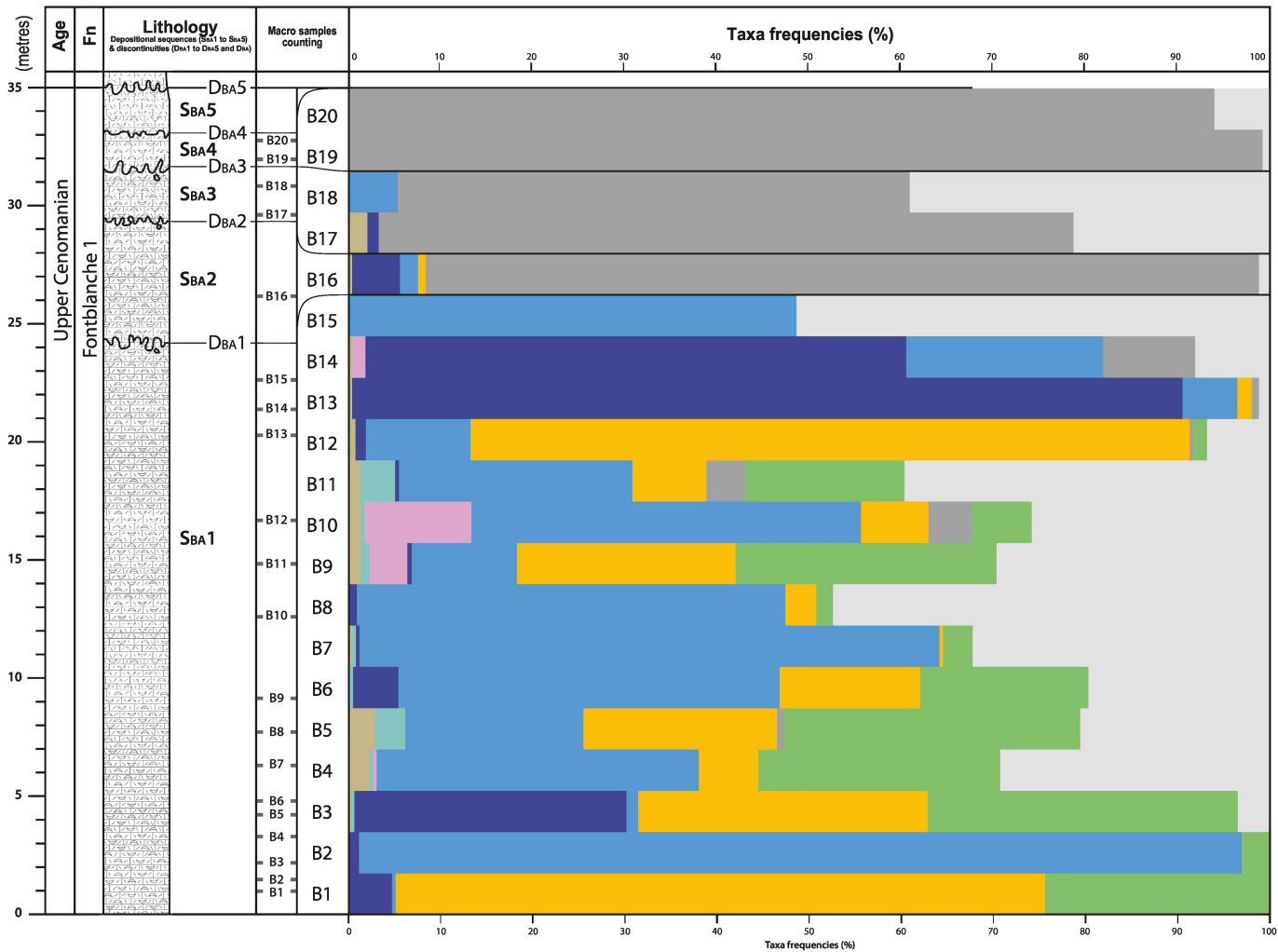
Figure 11

Figure 12

Figure 13